IEEE Access
Multidisciplinary | Rapid Review | Open Access Journal

Received May 6, 2022, accepted May 22, 2022, date of publication June 2, 2022, date of current version June 13, 2022.

Digital Object Identifier 10.1109/ACCESS.2022.3179688

An Aggregated Dynamic Model of an Electronically Actuated ICE Powertrain

SUBHADEEP KUMAR[1,2,3], RAMKRISHNA PASUMARTHY[1,2,3], (Member, IEEE), AND NIRAV P. BHATT[2,3,4], (Member, IEEE)

[1]Department of Electrical Engineering, Indian Institute of Technology Madras, Chennai 600036, India
[2]Robert Bosch Center for Data Science and Artificial Intelligence, Indian Institute of Technology Madras, Chennai 600036, India
[3]Prospective Center of Excellence for Network Systems Learning, Control and Evolution Group, Indian Institute of Technology Madras, Chennai 600036, India
[4]Department of Biotechnology, Indian Institute of Technology Madras, Chennai 600036, India

Corresponding author: Subhadeep Kumar (kr.subhadeepkumar@gmail.com)

This work was supported by the Science and Engineering Research Board Research Grant, Government of India (CRG/2020/005935).

ABSTRACT Electronically actuated systems in internal combustion engine (ICE) vehicles provide an opportunity for introducing partial autonomy in these vehicles. Controllers for total or partial autonomy of vehicle motion necessitate models of vehicular systems characterized by accurate transient and steady-state responses. We consider an ICE powertrain with a push belt type continuous variable transmission (CVT) associated with a double pinion planetary gear set. We propose a novel model for the planetary gear set as a differential-algebraic-equation (DAE) system with switching dynamics. We extend the dynamic torque converter model by incorporating the dynamics of the torque converter clutch with it. We combine CVT variator kinematics and dynamics of pulley motion and hydraulics and develop an aggregated model. Further, we construct data-driven models for the CVT's traction coefficient and equilibrium force ratio. To operate the CVT, we design a rule-based controller that makes the CVT function at discrete steady-state ratios. Furthermore, we provide a model of a directional control valve (DCV) to capture the partial flows during the transients of the DCV. We combine these models with the existing models of powertrain components and vehicle dynamics to study the utility of the proposed models. We consider three case study examples with realistic scenarios resembling vehicle maneuver in traffic, stop-and-go motion, and reverse motion to examine the models' ability to capture transient and steady-state characteristics and compare the resulting behaviour with the expected response.

INDEX TERMS Powertrain, automotive control, continuous variable transmission, planetary gear, vehicle dynamics.

I. INTRODUCTION

Modern internal combustion engine (ICE) vehicles consist of control-by-wire components to implement safety systems, assist systems, fuel optimization control systems, ride comfort control systems, etc. Most existing safety and driving assistance systems are limited to alerting drivers in adverse scenarios and do not take over the vehicle's control from the driver. The presence of active components in these vehicles provides an opportunity to introduce driving autonomy [1]. A vehicle model is essential for developing an autonomous control system that presides over human drivers [2]. The complexity of a vehicle model depends on the intended control application. For example, consideration of vehicle motion dynamics suffices to design controllers for driving assistance systems. In contrast, a controller for fuel optimization needs a model describing the powertrain and the vehicle motion. For designing self-driving controllers, models capturing the transient response of the vehicle and its underlying components are crucial in ensuring safe autonomous driving.

We focus on a powertrain with a push belt continuous variable transmission (CVT), commonly found in ICE vehicles nowadays. The powertrain comprises a spark-ignition engine, a torque converter, push belt CVT, a double pinion planetary gear system for the Drive-Neutral-Reverse operation, and required hydraulic components. The engine module is fitted with a linear actuator for torque assist and

The associate editor coordinating the review of this manuscript and approving it for publication was Shadi Alawneh.

the other components are operated using electro-hydraulic actuators. The linear actuator and the electro-hydraulic actuators allow to control the powertrain with voltage inputs. Existing literature provides detailed and well-established mathematical models of different automotive systems. Some noteworthy models are the torque converter model [3], engine model [4], steering model [5], Magic formula Tyre model [6], among several others. Models of planetary gear systems in the literature either ignore the transient characteristics [7] or involve a considerable number of degrees of freedom which is redundant for control applications [8], [9]. Analyzing the transient response of the planetary gears is crucial in determining appropriate inputs to other powertrain components. Additionally, an aggregated control-oriented model of a CVT describing the variator kinematics, pulley dynamics, and actuation mechanism cannot be found in the literature. Grey box models like the *CMM* model [10], *Shafai* model [11], *Ide* model [12], and white-box models in [13], [14] are available in the literature to model push belt and chain type CVTs. These models either focus on the variator's working principle or the pulleys' combined with approximated dynamics for the other aspects of the CVT. Apart from that, Hrovat's torque converter model [3] only provides dynamics for the hydrodynamic operation without a locking clutch. The model does not capture the dynamics for the locked mode of operation.

We put forth a novel model for a double pinion planetary gearbox in this work. The planetary system comprises a sun gear, a ring gear, a carrier, two planet gears, and two clutches for *Drive* and *Reverse* operations. The model describes the mechanism of the gearbox using differential-algebraic equations (DAE) with switching dynamics. It is shown how applied torque on the planetary gears affects the switching in the DAE system and results in a change of the algebraic variable. The CMM model for a chain pulley type CVT [10] is modified with rotational dynamics and other constraints. The dynamic torque converter model by Hrovat *et al.* [3] is adapted with the dynamics of torque converter clutch and actuator dynamics.

Usage of DCVs in hydraulic circuits for controlling fluid flow in CVT pulley cylinders can be found in [13]–[15]. In this work, we considered 3-way 3-position directional control valves (DCV) for controlling these hydraulic pressures. Existing simple models [13], [14] explains the flow dynamics at the steady-state positions of the valve spool and ignore the flows during the transient stage of the spool displacement. Detailed models such as those given in [16] require the determination of many parameters, which is difficult to obtain. We propose a model for the DCV considered capable of capturing the flows during both transient and steady-state operations.

We combine the developed models of the planetary gearbox, the CVT, the torque converter, and the DCV with the existing models of engine, engine actuator, clutch, and hydraulic systems to develop an aggregated powertrain model. We also develop a controller to determine the input voltages to the actuator for operating the CVT. To study the behaviour of the models, we assimilate the powertrain model with a brake model, Tyre model, wheel dynamics, and longitudinal dynamics of a vehicle. Finally, the following cases resembling realistic scenarios are studied to demonstrate the proposed models: (a) the maneuver of a vehicle in traffic, (b) stop and go characteristics of a vehicle, and (c) reverse motion. These case studies establish the proposed models' ability to capture the desired transient and steady-state responses by comparing the ICE powertrain's expected outcomes and features. The voltage inputs to the actuators are defined with a particular set of rules and in accordance with the case study scenarios and are explained in detail in Section XII.

The paper is organized as follows. Our contributions are briefly highlighted in Section II. The powertrain architecture is described in Section III. The extended model of the lockup torque converter is explained in Section IV. The planetary gearbox model is presented in Section V. The aggregated CVT model is explained in Section VI. The hydraulic circuit and the model for the DCV are described in Section VII. The aggregated powertrain model is summarized in Section VIII. The details of the models considered for the other powertrain components and the vehicle dynamics are given in Section IX. The CVT controller is described in Section X. Necessary details for the simulation studies are provided in Section XI. The case study examples are illustrated in Section XII, and Section XIII concludes the work.

II. MAIN CONTRIBUTIONS

We aim to develop a model-based controller for driving autonomy in ICE vehicles. This requires a model with the detailed dynamics of the vehicular systems and sub-systems. Developing a controller with a detailed complex can be challenging. The difficulty can be avoided by following a hierarchical approach with a distributed control strategy. Considering this control architecture to be utilized later, we developed the powertrain model. Our contributions are as follows:

- In the planetary gearbox model, we determine an algebraic constraint from the gear's angular velocities and use the Lagrange method to obtain their coupled dynamics. We integrate the algebraic constraint with the dynamics and model the system as a differential-algebraic equations (DAE) system. Further, we describe the change in the *Drive*, *Neutral*, and *Reverse* modes with switching dynamics. We show that changing the algebraic variable inhibits the switching of the system dynamics and successfully describes the operation of the planetary gearbox for all drive modes preserving the continuity of the system states.
- We combine the *CMM* model [10], pulleys' rotational and translational dynamics, dynamics of the hydraulics in the pulley cylinder. For the aggregation, we consider

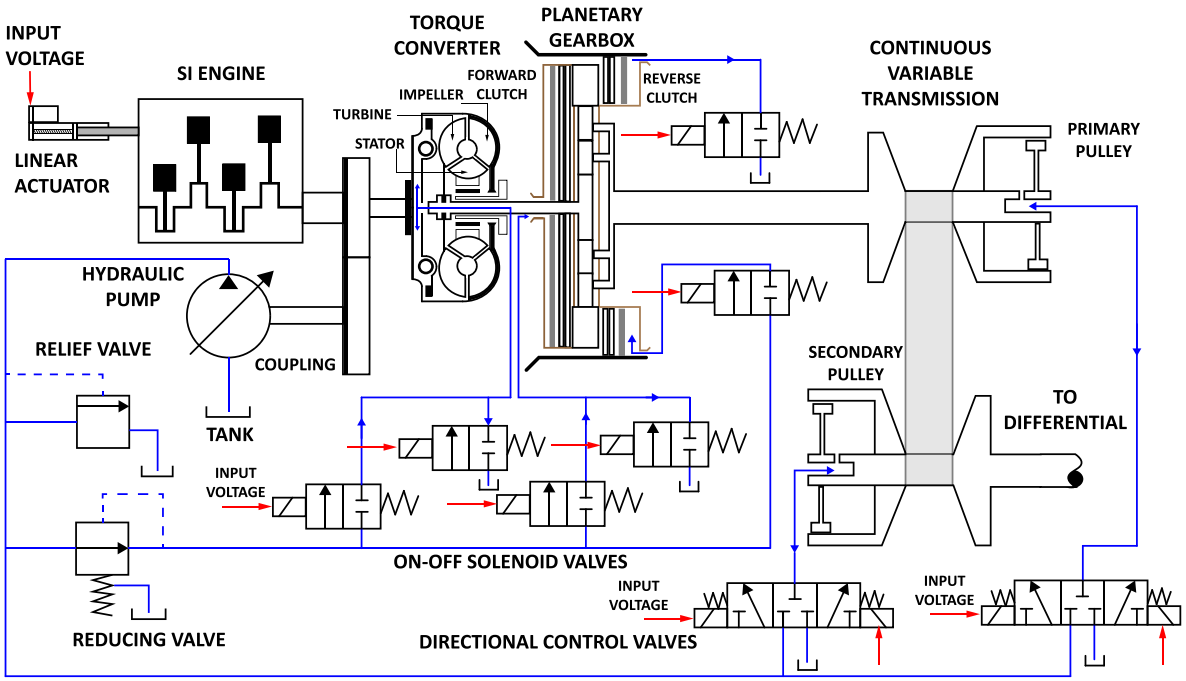

FIGURE 1. Schematic diagram of the powertrain.

the variator kinematics as an algebraic constraint and include the CVT dynamics to model the CVT as a DAE system. Further, we present data-driven models for the CVT's traction coefficient and equilibrium force ratio in the *CMM* model to complete the aggregated CVT model.

- Further, we integrate the dynamics of the torque converter clutch (TCC) and the clutch actuation dynamics with Hrovat's dynamic torque converter model [3]. To integrate the TCC's dynamics, we incorporate the frictional torque from the TCC and the load on the torque converter due to the TCC. To complete the model, we include the hydraulics in the TCC assembly with the fluid inflow and outflow as the control variables.
- In the proposed DCV model, we define nine modes of operation for the DCVs based on the spool position and determine the DCV's dynamics in these modes to incorporate the transient responses. The approach can also be used to model other DCVs and valves.
- We conceptualize a holistic powertrain model consisting of a spark ignition (SI) engine, a torque converter, a double-pinion planetary gear system, a pulley-type push belt CVT, and associated hydraulic systems and the corresponding electronically controlled actuators.
- Finally, we present a controller to operate the CVT at discrete steady-state transmission ratios and maintain its radii and pressure bounds.

III. POWERTRAIN ARCHITECTURE

In this paper, we consider a CVT-based powertrain whose components are actuated by electromechanical or electrohydraulic means. The powertrain is powered by a spark ignition (SI) engine where an electronic linear actuator controls the throttle. The transmission considered is a push belt type CVT. The CVT primary and secondary are shifted using directional control valves (DCV). A single-stage lockup torque converter is chosen for power transfer from the engine to the CVT. The torque converter clutch (TCC) operation is controlled using solenoid valves. A double pinion planetary gear set between the torque converter and CVT allows forward and reverse motion. The hydraulic actuation systems, a centrifugal gear pump powered by the SI engine and associated pressure valves, are the powertrain's hydraulic system elements. Hydraulics in the TCC and the planetary gear clutches are controlled by a set of ON-OFF solenoid valves for each clutch. The CVT pulley displacements are controlled using two 3-way 3-position directional control valves. The valves and the linear actuator are operated using voltage inputs. The hydraulic pressure is generated by a centrifugal pump, and the pressure is maintained with a pressure relief valve and a pressure reducing valve. The pump and the valves are the elements of the hydraulic system in the powertrain.

A schematic diagram of the powertrain is presented in Fig. 1.

IV. TORQUE CONVERTER

A lock-up torque converter operates in two modes - 1) the hydrodynamic mode, and 2) the locked mode. In the hydrodynamic mode, torque is transferred from the impeller to the turbine via fluid coupling. In the locked mode, the impeller and the turbine are connected mechanically via

a clutch. Engagement and disengagement of the lock-up clutch or the torque converter clutch (TCC) are controlled via an electro-hydraulic actuator. The dynamic model by Hrovat [3] is considered here, which helps in analyzing the operation of a torque converter with both transient and steady-state responses. In this work, the model of Hrovat [3] is extended with the dynamics of the TCC to incorporate the transient behaviour during locking and unlocking. With the dynamics of the TCC and its actuation, the dynamics during the transition between the hydrodynamic and locked modes are captured, and thus the continuity of the torque converter states is preserved. Next, the models describing the unlocked and locked models are presented.

Under the assumptions on fluid flow, effects of blade thickness, thermal effects made in [3], the dynamics of the lock-up torque converter for the unlocked modes are given by

$$\begin{aligned}
J_i\frac{\mathrm{d}\omega_i}{\mathrm{d}t}+\rho_{tc}S_iA_{tc}\frac{\mathrm{d}v_{tc}}{\mathrm{d}t} &= \tau_i-\tau_{i0}-\tau_{tcc} && \text{(1a)}\\
J_t\frac{\mathrm{d}\omega_t}{\mathrm{d}t}+\rho_{tc}S_tA_{tc}\frac{\mathrm{d}v_{tc}}{\mathrm{d}t} &= \tau_{t0}-\tau_t-B_{tc}\left(\omega_t-\omega_{tcc}\right)\\
&\quad -k_{tc}\left(\theta_t-\theta_{tcc}\right) && \text{(1b)}\\
J_s\frac{\mathrm{d}\omega_s}{\mathrm{d}t}+\rho_{tc}S_sA_{tc}\frac{\mathrm{d}v_{tc}}{\mathrm{d}t} &= \tau_s-\tau_{s0} && \text{(1c)}\\
J_{tcc}\frac{\mathrm{d}\omega_{tcc}}{\mathrm{d}t} &= \tau_{tcc}-B_{tc}\left(\omega_{tcc}-\omega_t\right)\\
&\quad -k_{tc}\left(\theta_{tcc}-\theta_t\right) && \text{(1d)}\\
S_i\frac{\mathrm{d}\omega_i}{\mathrm{d}t}+S_t\frac{\mathrm{d}\omega_t}{\mathrm{d}t}+S_s\frac{\mathrm{d}\omega_s}{\mathrm{d}t}+l_{tc}\frac{\mathrm{d}v_{tc}}{\mathrm{d}t} &= f_{tc}(\omega_i,\omega_t,\omega_s,v_{tc}) && \text{(1e)}
\end{aligned}$$

where the J's are the respective inertia, τ_j's are the external torque, τ_{j0}'s are the steady-state torque, and S's are the characteristic area constant of the impeller, turbine and stator, respectively. θ_{tcc}, τ_{tcc}, J_{tcc}, ω_{tcc}, B_{tc}, and k_{tc} represent the angular displacement, friction torque, inertia, angular velocity, damping coefficient and the spring constant of the torque converter clutch. Further, v_{tc}, ρ_{tc}, A_{tc} and l_{tc} denote the relative fluid velocity, fluid density in the torque converter, the cross-sectional area and effective fluid inertia length of the torque converter. The function $f_{tc}(\omega_i,\omega_t,\omega_s,v_{tc})$ in (1e) is a polynomial expression of the dependent variables, derived in [17].

During the hydrodynamic mode of operation, slight viscous friction is present between the clutch plates, which generates a small drag torque. In this work, we assume that the drag torque in the disengaged mode of operation is 0 as it is negligible compared to the torque transferred across the torque converter. The dynamics for the locked mode of operation can be written as

$$\begin{aligned}
\frac{\mathrm{d}\omega_i}{\mathrm{d}t} &= \frac{1}{J_i+J_{tcc}}\left(\tau_i-B_{tc}\left(\omega_i-\omega_t\right)-k_{tc}\left(\theta_i-\theta_t\right)\right) && \text{(2a)}\\
\frac{\mathrm{d}\omega_t}{\mathrm{d}t} &= -\frac{1}{J_t}\left(\tau_t+B_{tc}\left(\omega_t-\omega_i\right)+k_{tc}\left(\theta_t-\theta_i\right)\right) && \text{(2b)}
\end{aligned}$$

Therefore, switching between the modes occurs depending on the angular velocities of the lockup clutch and the impeller.

Here, the input torque at the impeller is the load torque at the engine, i.e., $\tau_i = \tau_{l_E}$, and the angular velocity of the impeller is equal to that of the engine, i.e., $\omega_i = \omega_e$.

A. TORQUE CONVERTER CLUTCH FRICTION

The torque converter clutch is a wet friction clutch that is engaged to transfer torque from the engine to the transmission with more significant efficiency. The engagement and disengagement of the clutch lead to a slip-stick behaviour which governs the friction torque generated in the clutch. Existing models for determining clutch friction torque considers either static or dynamic friction in the clutch plates [18]–[21]. A static clutch model is considered here with the Stribeck friction model. The clutch torque is given as

$$\begin{aligned}
\tau_{tcc} &= N_{tc}P_{tcc}A_{tcc}R_{e_{tcc}}\mu(\omega_{r_{tcc}})\mathrm{sgn}(\omega_{r_{tcc}})\\
R_{e_{tcc}} &= \frac{2}{3}\left(\frac{R_{o_{tcc}}^3-R_{i_{tcc}}^3}{R_{o_{tcc}}^2-R_{i_{tcc}}^2}\right)\\
A_{tcc} &= \pi\left(R_{o_{tcc}}^2-R_{b_{tcc}}^2\right)\\
\mu(\omega_{r_{tcc}}) &= \mu_{c_{tcc}}+\left(\mu_{s_{tcc}}-\mu_{c_{tcc}}\right)\exp\left(-\left|\frac{\omega_{r_{tcc}}}{\omega_{s_{tcc}}}\right|^{\lambda_{s_{tcc}}}\right)\\
&\quad +\beta_{v_{tcc}}\left|\omega_{r_{tcc}}\right|\\
\omega_{r_{tcc}} &= \omega_{tcc}-\omega_i
\end{aligned} \qquad (3)$$

where N_{tc}, A_{tcc}, $R_{o_{tcc}}$, $R_{i_{tcc}}$, and $R_{b_{tcc}}$ are the number of plates, piston area, outer radius, inner radius and bore radius of the torque converter clutch. $\mu(\cdot)$ gives the Stribeck friction where $\mu_{c_{tcc}}$, $\mu_{s_{tcc}}$, and $\beta_{v_{tcc}}$ are the Coulomb, Stribeck and viscous friction coefficient, respectively, and $\omega_{s_{tcc}}$, $\lambda_{s_{tcc}}$ are the Stribeck friction coefficients for the torque converter clutch.

B. DYNAMICS OF THE CLUTCH ASSEMBLY

The piston pressure (P_{tcp}) and velocity (v_{tcp}) dynamics in the clutch assembly are given by [22]

$$\begin{aligned}
\frac{\mathrm{d}P_{tcp}}{\mathrm{d}t} &= \frac{B_{hyd}}{V_{tcp}+A_{tcp}s_{tcp}}\left(Q_{tc_o}-Q_{tc_{in}}-A_{tcp}v_{tcp}\right) && \text{(4a)}\\
\frac{\mathrm{d}v_{tcp}}{\mathrm{d}t} &= \frac{1}{M_{tcp}}\left(F_{spr_{tcp}}-D_{tcp}v_{tcp}-F_{sl_{tcp}}\mathrm{sgn}(v_{tcp})\right.\\
&\quad \left.-A_{tcp}\left(P_{tcp}+P_{cf_{tcc}}\right)\right) && \text{(4b)}
\end{aligned}$$

where B_{hyd} is the bulk modulus of the automatic transmission fluid (ATF) and $Q_{tc_{in}}$, Q_{tc_o} are the inflow and the outflow rates of the ATF in the TCC piston chamber. The other symbols have their usual meaning, and the subscript *tcp* denotes the TCC piston.

As the clutch assembly rotates, a centrifugal force is exerted on the clutch disks. The equivalent pressure, $P_{cf_{tcc}}$, due to the centrifugal force, depends primarily on the angular velocity of the clutch assembly as well as the fluid level height in the piston assembly, $R_{st_{tcp}}$. The pressure generated due to

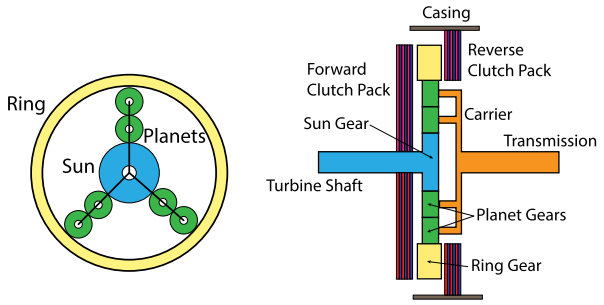

FIGURE 2. Schematic of the planetary gear set.

the centrifugal force, $P_{cf_{tcc}}$, is expressed as

$$P_{cf_{tcc}} = \frac{\pi \rho_{hyd} \omega_{tcc}^2}{A_{tcp}} \left(\frac{1}{4} \left(R_{o_{tcc}}^4 - R_{i_{tcc}}^4 \right) - \frac{1}{2} \left(R_{st_{tcp}}^2 \left(R_{o_{tcc}}^2 - R_{i_{tcc}}^2 \right) \right) \right) \quad (5)$$

Finally, the piston seal drag force is given by [23]

$$F_{sl_{tcp}} = \left(k_{s_{tcp}} \left(P_{tcp} + P_{cf_{tcc}} \right) + C_{1_{tcp}} \right) \tanh \frac{v_{tcp}}{C_{2_{tcp}}} \quad (6)$$

where $k_{s_{tcp}}$ is the static frictional resistance coefficient of the clutch piston and $C_{1_{tcp}}$, $C_{2_{tcp}}$ are constant terms.

V. PLANETARY GEARBOX

A double pinion planetary gear set is considered here along with a clutch pack for drive and reverse mode. Fig. 2 depicts the planetary gear system considered. The gear system comprises a sun gear, a ring gear, a carrier and six planet gears. The sun gear connects the turbine shaft while the carrier connects the CVT primary pulley. In the *Neutral* mode, both the clutch packs remain disengaged. When the gear mode is changed from *Neutral* to *Drive*, the forward clutch pack is engaged, while the reverse clutch pack is engaged for the *Reverse*. As the separator disks and the friction disks are pressed in the forward clutch pack, the generated friction torque gradually adjusts the velocities in the sun and the ring gear, allowing them to rotate at the same angular velocity. Similarly, the reverse clutch mechanically connects the clutch housing and the ring gear, restricting any rotational motion. The kinematics of the angular velocities in the planet gears can be written as

$$\omega_{p_1} R_{p_1} = -\omega_{sg} R_{sg} + \omega_c R_{sg} \quad (7a)$$
$$\omega_{p_2} R_{p_2} = \omega_{rg} R_{rg} - \omega_c R_{rg} \quad (7b)$$
$$\omega_{p_1} R_{p_1} = -\omega_{p_2} R_{p_2} \quad (7c)$$

where ω_{p_i} $(i = 1, 2)$ are the angular velocities of the planet gears, $i = 1$ and $i = 2$ denote the pinions adjacent to the sun and ring gear, respectively and R_{p_i} is the pinion radius in the i^{th} level. The subscripts sg, rg and c represent the sun gear, ring gear and carrier, respectively. Solving (7), we get

$$\omega_c (R_{rg} - R_{sg}) = \omega_{rg} R_{rg} - \omega_{sg} R_{sg} \quad (8)$$

The algebraic relations of the gear's angular velocities in (8) govern the dynamics of the planetary gear set. The kinetic energies, K_i $(i = \{sg, rg, c\})$, of the sun gear, ring gear, and the carrier is obtained as:

$$K_i = \frac{1}{2} J_i \omega_i^2, \quad i = \{sg, rg, c\} \quad (9)$$

where J_i $(i = \{sg, rg, c\})$ is the moment of inertia of the respective gear. Similarly, the kinetic energies of the planet gears can be obtained as:

$$K_{p_1} = \frac{n_p}{2} \left(J_{p_1} \omega_{p_1}^2 + M_{p_1} \left(R_{p_1} + R_{sg} \right)^2 \omega_c^2 \right)$$
$$K_{p_2} = \frac{n_p}{2} \left(J_{p_2} \omega_{p_2}^2 + M_{p_2} \left(R_{p_1} + R_{p_2} + R_{sg} \right)^2 \omega_c^2 \right) \quad (10)$$

where n_p is the number of planet gears in each level, J_{pi1}, J_{pi2} are the respective moment of inertia, and M_{pi1}, M_{pi2}, are the respective masses. Here, $n_p = 3$. Assume that there are no linear displacements along either axis of the gears, the system's potential energy remains unchanged, i.e., $\mathcal{V} = 0$. Therefore, the Lagrangian function for the planetary system is given by

$$\mathcal{L} = \mathcal{K} - \mathcal{V} = K_{sg} + K_{rg} + K_c + \sum_{i=1}^{3} K_{pi1} + \sum_{i=1}^{3} K_{pi2} \quad (11)$$

Let the external torques and virtual displacements on the sun gear, ring gear and the carrier be $\tau_i (i = \{sg, rg, c\})$ and $\delta\theta_i (i = \{sg, rg, c\})$, respectively. Then, the work done by the planetary gear system on application of the external torque is

$$\delta W = \tau_{sg} \delta\theta_{sg} + \tau_{rg} \delta\theta_{rg} + \tau_c \delta\theta_c \quad (12)$$

Hence, the system of the planetary gear set is essentially a *DAE* system with two differential state variables and $2n_p + 1$ algebraic variables.

A. DYNAMICS 1

Considering the algebraic constraint in (8) and choosing the degrees of freedom to be θ_{sg} and θ_{rg}, (12) can be re-written as

$$\delta W = \left(\tau_{sg} - \frac{R_{sg}}{R_{sg} + R_{rg}} \tau_c \right) \delta\theta_{sg} + \left(\tau_{rg} + \frac{R_{rg}}{R_{sg} + R_{rg}} \tau_c \right) \delta\theta_{rg} \quad (13)$$

Therefore, the equations of motion obtained using the D'Alembert's principle are

$$\frac{\mathrm{d}}{\mathrm{d}t} \left(\frac{\partial \mathcal{L}}{\partial \omega_{sg}} \right) - \frac{\partial \mathcal{L}}{\partial \theta_{sg}} = \tau_{sg} - \frac{R_{sg}}{R_{sg} + R_{rg}} \tau_c \quad (14a)$$
$$\frac{\mathrm{d}}{\mathrm{d}t} \left(\frac{\partial \mathcal{L}}{\partial \omega_{rg}} \right) - \frac{\partial \mathcal{L}}{\partial \theta_{rg}} = \tau_{rg} + \frac{R_{rg}}{R_{sg} + R_{rg}} \tau_c \quad (14b)$$

Using (7-11) in (14), we get

$$c_1 \frac{\mathrm{d}\omega_{sg}}{\mathrm{d}t} + c_2 \frac{\mathrm{d}\omega_{rg}}{\mathrm{d}t} = \tau_{sg} - \frac{R_{sg}}{R_{sg} + R_{rg}} \tau_c \quad (15a)$$
$$c_2 \frac{\mathrm{d}\omega_{sg}}{\mathrm{d}t} + c_3 \frac{\mathrm{d}\omega_{rg}}{\mathrm{d}t} = \tau_{rg} + \frac{R_{rg}}{R_{sg} + R_{rg}} \tau_c \quad (15b)$$

where

$$c_1 = J_{sg} + \frac{R_{sg}^2}{R_{pg}^2}\left(J_p^\star + R_{rg}^2 \sum_{i=1}^{2} \frac{J_{p_i}}{R_{p_i}^2} + \frac{J_c}{n_p}\right)$$

$$c_2 = -\frac{R_{rg}R_{sg}}{R_{pg}^2}\left(J_p^\star + R_{rg}R_{sg} \sum_{i=1}^{2} \frac{J_{p_i}}{R_{p_i}^2} + \frac{J_c}{n_p}\right)$$

$$c_3 = J_{rg} + \frac{R_{rg}^2}{R_{pg}^2}\left(J_p^\star + R_{sg}^2 \sum_{i=1}^{2} \frac{J_{p_i}}{R_{p_i}^2} + \frac{J_c}{n_p}\right)$$

$$R_{pg} = \frac{1}{\sqrt{n_p}}\left(R_{rg} - R_{sg}\right)$$

$$J_p^\star = M_{p_1}(R_{p_1} + R_{sg})^2 + M_{p_2}(R_{p_1} + R_{p_2} + R_{sg})^2$$

For the powertrain considered, $\tau_{sg} = \tau_t$, $w_{sg} = w_t$, $w_c = w_{p_{cvt}}$ and $\tau_c = \tau_{p_{cvt}}$ where $w_{p_{cvt}}$ and $\tau_{p_{cvt}}$ are the angular velocity and torque supplied to the primary pulley of the CVT, respectively.

B. DYNAMICS 2

However, when both the clutches are disengaged, i.e. in the *Neutral* mode, the choice of degrees of freedom to determine the expression for virtual work in (13) does not help in determining the dynamics. In the *Neutral* mode, the external torque acts on either the sun gear or the carrier or both of them. Therefore, the suitable choice for degrees of freedom is θ_{sg} and θ_c. The switching of modes occurs at the zero-crossing of the external torque on the ring gear, τ_{rg}. In this mode, when the vehicle is at rest, i.e. $\omega_c = 0$, the relation between the angular velocity of the sun gear and ring gear are derived from the algebraic constraint (8) as

$$\omega_{rg} = \omega_{sg}\frac{R_{sg}}{R_{rg}} \tag{16}$$

and the rotational dynamics of the sun gear is given by

$$\frac{\mathrm{d}\omega_{sg}}{\mathrm{d}t} = \frac{\tau_{sg}}{J_{sg} + \frac{R_{sg}^2}{R_{p_1}^2}n_p J_{p_1} + \frac{R_{sg}^2}{R_{p_2}^2}n_p J_{p_2} + \frac{R_{sg}^2}{R_{rg}^2}J_{rg}} \tag{17}$$

Cars are provided with parking brakes which prevent any unwanted movement of a vehicle while parked. When parking brakes are not applied, the wheels may rotate due to external force even though the vehicle is kept in *Neutral*, such as gravitational pull in an incline. In such scenarios, the rotational dynamics of the gears can be derived using the same method as shown in (13)-(15), considering θ_{sg} and θ_c as the degrees of freedom. The equations of rotation are given by:

$$c_4\frac{\mathrm{d}\omega_{sg}}{\mathrm{d}t} + c_5\frac{\mathrm{d}\omega_c}{\mathrm{d}t} = \tau_{sg} \tag{18a}$$

$$c_5\frac{\mathrm{d}\omega_{sg}}{\mathrm{d}t} + c_6\frac{\mathrm{d}\omega_c}{\mathrm{d}t} = \tau_c \tag{18b}$$

where

$$c_4 = J_{sg} + J_{rg}\frac{R_{sg}^2}{R_{rg}^2} + n_p R_{sg}^2 \sum_{i=1}^{2} \frac{J_{p_i}}{R_{p_i}^2}$$

$$c_5 = J_{rg}\left(\frac{R_{sg}(R_{rg} - R_{sg})}{R_{rg}^2}\right) - n_p R_{sg}^2 \sum_{i=1}^{2} \frac{J_{p_i}}{R_{p_i}^2}$$

$$c_6 = J_c + n_p\left(J_p^\star + R_{sg}^2 \sum_{i=1}^{2} \frac{J_{p_i}}{R_{p_i}^2}\right) + J_{rg}\frac{(R_{rg} - R_{sg})^2}{R_{rg}^2}$$

However, if the engine is turned off, then $\omega_{sg} = 0$ and the algebraic constraint in (8) gives $\omega_{rg} = \omega_c\frac{R_{rg}-R_{sg}}{R_{rg}}$. Then, the rotational dynamics of the carrier is given by

$$\frac{\mathrm{d}\omega_c}{\mathrm{d}t} = \frac{\tau_c}{J_c + \frac{R_{sg}^2}{R_{p_1}^2}n_p J_{p_1} + \frac{R_{sg}^2}{R_{p_2}^2}n_p J_{p_2} + \frac{R_{pg}^2}{R_{rg}^2}n_p J_{rg}} \tag{19}$$

C. CLUTCH TORQUE AND CLUTCH DYNAMICS

External torque is applied to the ring gear upon engagement of either clutch packs, which can be written as

$$T_{rg} = \begin{cases} B_{fc}\Delta\omega_{fc}^{sg} + k_{fc}\Delta\theta_{fc}^{sg} - \mathrm{sgn}\left(\Delta\omega_{rc}^{rg}\right)\tau_{rc}, \\ \qquad\qquad \text{forward clutch stick} \\ -\mathrm{sgn}\left(\Delta\omega_{fc}^{rg}\right)\tau_{fc} - \mathrm{sgn}\left(\Delta\omega_{rc}^{rg}\right)\tau_{rc}, \\ \qquad\qquad \text{slip or slip-stick} \\ -\mathrm{sgn}\left(\Delta\omega_{fc}^{rg}\right)\tau_{fc} - B_{rc}\omega_{rc} - k_{rc}\theta_{rc}, \\ \qquad\qquad \text{reverse clutch stick} \end{cases} \tag{20}$$

where $\Delta\omega_q^p = \omega_p - \omega_q$, $\Delta\theta_q^p = \theta_p - \theta_q$ ($p = \{sg, rg\}$, $q = \{fc, rc\}$) and the subscripts 'fc' and 'rc' represent forward and reverse clutch pack, respectively. B_i, k_i, θ_i, ω_i, τ_i ($i = \{fc, rc\}$), are the torsional damping, torsional stiffness, angular displacement, angular velocity and friction torque in the clutches. The friction torque can be modeled using static or dynamic friction in the clutch plates [19]–[21].

The rotational dynamics of the clutches is given by

$$J_{fc}\frac{\mathrm{d}\omega_{fc}}{\mathrm{d}t} = \mathrm{sgn}\left(\Delta\omega_{fc}^{rg}\right)\tau_{fc} + B_{fc}\Delta\omega_{fc}^{sg} + k_{fc}\Delta\theta_{fc}^{sg}$$

$$J_{rc}\frac{\mathrm{d}\omega_{rc}}{\mathrm{d}t} = \mathrm{sgn}\left(\Delta\omega_{rc}^{rg}\right)\tau_{rc} - B_{rc}\omega_{rc} - k_{rc}\theta_{rc} \tag{21}$$

where J_{fc} and J_{rc} are the moment of inertia of the forward clutch and reverse clutch, respectively. The clutch actuation dynamics comprises the dynamics of the hydraulic pressure in the piston assembly and the translation of the piston. The clutch actuation dynamics follows the same dynamics as depicted in (4), (5) and (6).

VI. CONTINUOUS VARIABLE TRANSMISSION

A pulley-type push belt CVT is considered for the powertrain model in this work. The primary pulley is connected to the planetary gear set's carrier, and the secondary pulley is connected to the differential via the propeller shaft. Axial clamping forces are applied on the pulleys, which changes the pulley radii, and as a result, the gear ratio changes.

The axial displacements of the pulley sheaves are controlled by electro-hydraulic actuators.

A. CVT CONSTRAINTS

The *geometric* ratio, *speed* ratio and *relative slip* of a CVT are defined as

$$r_{g_{cvt}} = \frac{R_{p_{cvt}}}{R_{s_{cvt}}}, \quad r_{s_{cvt}} = \frac{\omega_{s_{cvt}}}{\omega_{p_{cvt}}}, \quad \nu_{cvt} = 1 - \frac{r_{s_{cvt}}}{r_{g_{cvt}}},$$

respectively, where $R_{p_{cvt}}$, $R_{s_{cvt}}$ are the radius and $\omega_{p_{cvt}}$, $\omega_{s_{cvt}}$ are the angular velocities of the primary and secondary pulley. The kinematics of the CVT originating from its geometric relation can be written as

$$\begin{aligned} L_{cvt} &= 2d_{cvt}\cos(\phi_{cvt}) + R_{p_{cvt}}\phi_{p_{cvt}} + R_{s_{cvt}}\phi_{s_{cvt}} \\ \phi_{cvt} &= \arcsin\left(\frac{R_{p_{cvt}} - R_{s_{cvt}}}{d_{cvt}}\right), \\ \phi_{p_{cvt}} &= \pi + 2\phi_{cvt}, \ \phi_{s_{cvt}} = \pi - 2\phi_{cvt} \end{aligned} \tag{22}$$

where L_{cvt} is the total length of the CVT belt, d_{cvt} is the center-to-center distance of the pulleys, and $\phi_{p_{cvt}}, \phi_{s_{cvt}}$ are the primary and secondary angle of wrap. The algebraic constraint in (22) holds under the assumption that there is no spiral motion in the belt, and hence the belt runs at a constant radius over the entire angle of wrap at each pulley.

A necessary criterion for torque transfer from the CVT primary to the secondary is that the belt should remain adhered to the pulleys. Hence, the pressure in the pulley cylinders should ensure that the clamping forces on the movable pulley sheaves are always greater or equal to the minimum value. This criterion can be expressed as constraints on the clamping forces ($F_{i_{cvt}}$), as

$$\begin{aligned} F_{i_{cvt}} &\geq \min\left(F_{p_{cvt}}, F_{s_{cvt}}\right) \\ &= \frac{\left|\tau_{i_{cvt}}\right|\cos(\beta_{cvt})}{2R_{i_{cvt}}\mu_{cvt}(\nu_{cvt})}, \quad i \in \{p, s\} \end{aligned} \tag{23}$$

where $\tau_{p_{cvt}}$ and $\tau_{s_{cvt}}$ are the torques exerted by the belt on the primary and secondary pulley, respectively, and μ_{cvt} is the traction coefficient at the pulleys. For ensuring minimum clamping force, the secondary pulley is supplemented with an additional spring. Assuming the spring force is linearly related to the spring displacement, the clamping forces on the pulleys can be written as

$$\begin{aligned} F_{p_{cvt}} &= A_{p_{cvt}}P_{p_{cvt}} + c_{fp_{cvt}}\omega_{p_{cvt}} \\ F_{s_{cvt}} &= A_{s_{cvt}}P_{s_{cvt}} + c_{fp_{cvt}}\omega_{s_{cvt}} + F_{ks0_{cvt}} \\ &\quad + k_{s_{cvt}}x_{s_{cvt}} \end{aligned} \tag{24}$$

where $A_{i_{cvt}}$s are the piston areas, $c_{fi_{cvt}}$s are the centrifugal force coefficients of the pulleys and $P_{i_{cvt}}$s are the pressure exerted on the pulleys. Further, $F_{ks0_{cvt}}$ is the pre-load force of the spring and $k_{s_{cvt}}$ is the spring constant. It is coherent that for torque transfer, the relative slip must not become zero, i.e., $r_{s_{cvt}} \neq r_{g_{cvt}}$. Therefore, the clamping forces are to be determined such that the constraint $\nu_{cvt} \neq 0$ holds. The relation between the pulley radii and the pulley displacements $x_{i_{cvt}}$ ($i \in \{p, s\}$) caused by the clamping forces can be obtained using the CVT geometry as

$$x_{i_{cvt}} = 2\tan(\beta_{cvt})\left(R_{i_{cvt}} - R_{i_{cvt}|min}\right), \ i \in \{p, s\}, \tag{25}$$

where β_{cvt} represents the pulley wedge angle, and $R_{i_{cvt}|min}$'s are the minimum radii.

An electro-hydraulic actuation mechanism is considered for controlling the pulley sheaves' axial displacements. The inputs to the pulley cylinders are the fluid input flow rates controlled by directional control valves, described in Section VII-A. The dynamics of the hydraulic pressures in the pulley cylinders follow from [14].

B. VARIATOR DYNAMICS

Altogether, the CVT variator dynamics can be modeled with the dynamics of the angular velocity and radius of the secondary pulley, the algebraic constraint in (22), and the inequality constraint in (23). However, due to pulley deformation, deflections in the belt, compression of the metal blocks, slip, etc., the clamping force does not control the shifting of the radius in all conditions, specifically in cases of macro slip. Here, the CMM model is considered for modeling the dynamics of the geometric ratio of the CVT, which highlights both the micro-slip and macro-slip properties of a CVT. The dynamics of the geometric ratio is given by:

$$\begin{aligned} \frac{\mathrm{d}r_{g_{cvt}}}{\mathrm{d}t} &= \omega_{DR}\Delta_{cvt}(F_{DN})\left(\frac{1+\cos^2(\beta_{cvt})}{\sin(2\beta_{cvt})}\right) \\ &\quad \cdot f_{cvt}\left(r_{g_{cvt}}\right)\ln\left(\frac{F_{DR}}{F_{DN}} - \frac{F_{DR|eq}}{F_{DN|eq}}\right) \\ f_{cvt}\left(r_{g_{cvt}}\right) &= r_{g_{cvt}}\frac{R_{DR_{cvt}}}{d_{cvt}}\left(F_{1_{cvt}} + F_{2_{cvt}}\ln\left(r_{g_{cvt}}\right)^2\right) \end{aligned} \tag{26}$$

The subscripts *DR* and *DN* represent the driving pulley and the driven pulley, respectively. Δ_{cvt} is a factor originating due to the deformation in pulleys and is dependent on the clamping force on the driven pulley. $F_{1_{cvt}}$ and $F_{2_{cvt}}$ are constants in the function f_{cvt}, which are to be determined using measurements. Hence, the variator dynamics can be described considering $\omega_{s_{cvt}}$ and $r_{g_{cvt}}$ as the differential states, and either of the pulley radii as the algebraic state.

C. ROTATIONAL DYNAMICS

The rotational dynamics of the primary pulley are the same as the carrier of the planetary gear set. If the torque losses and the inertia effects of the belt are neglected, then the rotational dynamics of the secondary pulley is given by

$$\begin{aligned} J_{s_{cvt}}\frac{\mathrm{d}\omega_{s_{cvt}}}{\mathrm{d}t} &= \frac{1}{r_{g_{cvt}}}\tau_{s_{cvt}} - \tau_d \\ \tau_{s_{cvt}} &= \frac{1}{r_{g_{cvt}}}\tau_{p_{cvt}} \\ &= \frac{2\mu_{cvt}(\nu_{cvt})R_{p_{cvt}}\min\left(F_{p_{cvt}}, F_{s_{cvt}}\right)}{r_{g_{cvt}}\cos(\beta_{cvt})} \end{aligned} \tag{27}$$

where τ_d is the load torque from the differential, and $J_{s_{cvt}}$ is the inertia of the secondary pulley.

D. CVT's TRACTION COEFFICIENT AND EQUILIBRIUM FORCE RATIO

In the CVT model, it is difficult to ascertain the factors that affect the equilibrium forces ($F_{DR|eq}, F_{DN|eq}$) and the traction coefficient (μ_{cvt}), through a first-principles analysis. Alternatively, it is possible to develop data-driven models among these variables and the primary variables that can be measured directly. The traction coefficient in the CVT, μ_{cvt}, depends explicitly on the slip ratio ν_{cvt}. Different functions were fitted to model the dependency of μ_{cvt} on ν_{cvt}. The function that gives the best fit is similar to the Magic formula Tyre model, given by

$$\mu_{cvt} = D_{cvt} \sin\big(C_{cvt} \arctan\big(B_{cvt}\nu_{cvt} - E_{cvt} \cdot \big(B_{cvt}\nu_{cvt} - \arctan\big(B_{cvt}\nu_{cvt}\big)\big)\big)\big) \quad (28)$$

The slip and friction in the CVT originate due to relative motion between the pulley sheaves and the variator exhibits similar phenomena of friction and slip in the tyres. Hence, a choice of a function similar to the magic formula is justified. The coefficients B_{cvt}, C_{cvt}, D_{cvt} and E_{cvt}, are determined by fitting test data with the function in (28) using the Least-squares Regression method. The coefficient values from the fitted model are $B_{cvt} = 1.6359$, $C_{cvt} = 0.14978$, $D_{cvt} = 0.7195$ and $E_{cvt} = 1.0308$. It is mention-worthy that the fitting is done based upon the mean of the friction values collected for three values of secondary pulley pressure, $P_{s_{cvt}}$. A better approximation function may be obtained considering the effect of the secondary pulley pressure.

Similarly, for the equilibrium forces, a model is fitted where κ_{cvt} gives the ratio of the equilibrium forces $\big(\kappa_{cvt} = F_{DR|eq}/F_{DN|eq}\big)$. Upon inspection, the equilibrium force ratio is found to depend upon the geometric ratio ($r_{g_{cvt}}$), the secondary pulley pressure ($P_{s_{cvt}}$), and the angular velocity of the secondary pulley ($\omega_{s_{cvt}}$). From the measurement data, the effects of the angular velocities of the secondary pulley are found to be insignificant and therefore mean values of κ_{cvt} over a range of $\omega_{s_{cvt}}$ are taken into consideration. Several functions are chosen to fit a model where κ_{cvt} depends on $r_{g_{cvt}}$ and $P_{s_{cvt}}$. The best fit is obtained for the function given by:

$$\begin{aligned}\kappa_{cvt} = {} & \big(1 + \exp\big(-\big(B_{3_{cvt}}P_{s_{cvt}}^2 + B_{2_{cvt}}P_{s_{cvt}} \\ & + B_{1_{cvt}}\big)\big(r_{g_{cvt}} + C_{1_{cvt}} + C_{2_{cvt}}P_{s_{cvt}}\big)\big)^{-1} \\ & \cdot \big(A_{1_{cvt}} + A_{2_{cvt}}P_{s_{cvt}} + A_{3_{cvt}}P_{s_{cvt}}^2\big) \\ & + \big(D_{1_{cvt}} + D_{2_{cvt}}P_{s_{cvt}} + D_{3_{cvt}}P_{s_{cvt}}^2\big) \\ & \cdot \big(r_{g_{cvt}}C_{1_{cvt}} + C_{2_{cvt}}P_{s_{cvt}}\big) - \frac{1}{2}\big(A_{1_{cvt}} \\ & + A_{2_{cvt}}P_{s_{cvt}} + A_{3_{cvt}}P_{s_{cvt}}^2\big) + E_{1_{cvt}} \\ & + E_{2_{cvt}}P_{s_{cvt}} \end{aligned} \quad (29)$$

The coefficients are obtained using the Least-squares Regression method, presented in Table 1.

TABLE 1. Coefficients of the fitted model for κ_{cvt}.

Coefficient	Value	Coefficient	Value
$A_{1_{cvt}}$	1.325	$A_{2_{cvt}}$	-5.953×10^{-7}
$A_{3_{cvt}}$	8.05×10^{-14}	$B_{1_{cvt}}$	7.171
$B_{2_{cvt}}$	2.563×10^{-6}	$B_{3_{cvt}}$	-2.495×10^{-13}
$C_{1_{cvt}}$	-0.934	$C_{2_{cvt}}$	2.02×10^{-8}
$D_{1_{cvt}}$	-0.1608	$D_{2_{cvt}}$	2.089×10^{-7}
$D_{3_{cvt}}$	-2.41×10^{-13}	$E_{1_{cvt}}$	1.0064
$E_{2_{cvt}}$	-2×10^{-8}		

VII. HYDRAULICS

Hydraulic circuits associated with an automotive powertrain consist of numerous components and display complex behaviour. In this work, part of the hydraulic circuit essential for the hydraulic operations in the powertrain is considered. The hydraulic circuit comprises a centrifugal gear pump, a pressure relief valve, a pressure reducing valve, two directional control valves (DCV), and six proportional solenoid valves. The engine powers the centrifugal gear pump, and the fluid pressure at the pump head is limited by using a pressure relief valve. The centrifugal pump pumps the ATF to the piston chambers in the clutch assemblies and the pulley cylinders in the CVT. The solenoid valves control the fluid flow in and out of the piston chambers, and the DCVs regulate the inflow and outflow in the pulley cylinders. The supply pressures to the solenoid valves are limited by a pressure reducing valve to avoid mechanical damage and wear. Cooling systems, accumulators, and other hydraulic components are ignored here. The schematic of the hydraulic circuit is shown in Fig. 1.

The following assumptions are made for the hydraulic system:

1) The tank pressure (P_{tank}) is equal to atmospheric pressure.
2) Hydraulic pressure across the accessory components such as cooler and filter is constant.
3) The hydraulic capacitance of the pipelines is time-invariant, and there is no pressure drop across the pipelines.
4) The discharge coefficient of the hydraulic components is constant.
5) The ATF's fluid density (ρ_{hyd}) and dynamic viscosity (μ_{hyd}) are time-invariant due to the fixed temperature of the ATF.
6) Mechanical compliance of the valve spools is time-invariant.
7) None of the valves has any flow force compensation.

A centrifugal gear pump is considered here. The empirical model of a centrifugal gear pump, developed by D. R. Grandall [24] is used for the powertrain model.

A. PROPORTIONAL DIRECTION CONTROL VALVE

In this hydraulic circuit, there is a 3-way 3-position DCV at each pulley cylinder, as shown in Fig. 1. The application of voltage on either of the solenoid displaces the DCV spool resulting in three steady-state modes of operation (i) *fill* mode: the valves allow ATF to flow from the pump to the cylinders in this mode, (ii) *hold* mode: the valves restrict all

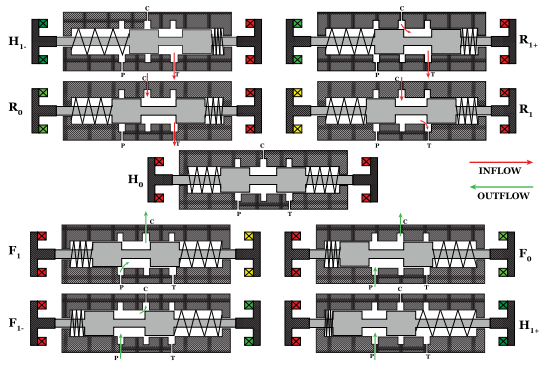

FIGURE 3. Modes of operation of the 3/3 proportional direction control valve.

fluid flow in this mode, and (iii) *release* mode: the valves allow to drain the cylinders to the tank in this mode.

First principle models of spool valves are developed by considering valve pressure, spool displacement, and velocity as the system states [14], [25]. The operation of the spool valve is expounded with the number of positions of the valves. The number of valve positions indicates the number of positions in which the valve operates in a steady state. As a result, the partial fluid flows and their effects during the transient stages are ignored. Without the transient stages, the hydraulic pressures of the CVT's pulley cylinder are discontinuous and hence the CVT's geometric ratio becomes discontinuous. We developed a detailed model with both the steady-state and transient characteristics of the 3-way 3-position DCVs.

The total length of the valve (L_{valve}) and the length of the rod (L_{rod}) are related to the length of the spool land (L_{land}), flow length (L_{flow}), and width of the ports (w_{port}) as

$$L_{valve} > 2L_{flow} + 2L_{land} + w_{port}, \text{ and,} \tag{30a}$$
$$L_{rod} > L_{flow}. \tag{30b}$$

Considering the relations in (30), a model is developed with nine modes of operation, three sub-modes each for *fill*, *release*, and *hold*. A pictorial overview of the 9 modes of operation is shown in Fig. 3. Let the length of the spring chambers be defined as L_{spr}. Then, if the displacement of the spool (s_i) is measured w.r.t the right end of the valve, the modes can be classified as shown in Table 2. The symbols H, F, and R, denote *hold*, *fill* and *release* modes of operation in the DCVs. The subscripts 0 and 1 indicate the ATF flows freely and partially across the valve ports, respectively, in the corresponding mode. The following $\pm$ sign in the subscripts denotes the secondary flow in and out of the spring chambers. If only (30a) is satisfied, then modes H_{1+} and H_{1-} do not exist. If the length L_{valve} is reduced to the extent such that both (30a) and (30b) are violated, and $L_{valve} = 2(L_{flow} + L_{land}) + w_{port}$, then only modes R_0 to F_0 exist. The valves are designed and calibrated to minimize the secondary flows. Any change in the pressures of the spring chambers gets adjusted due to leakage flow in the valve.

TABLE 2. Proposed modes of the 3-way 3-position direction control valve.

Mode	Condition
H_{1+}	$s_i < L_{spr_i} + L_{flow_i} - L_{rod_i} - L_{land_i} - \frac{1}{2}w_{port_i}$
R_{1+}	$-\frac{1}{2}w_{port_i} \leq s_i - L_{spr_i} - L_{flow_i} + L_{rod_i} + L_{land_i} < \frac{1}{2}w_{port_i}$
R_0	$L_{flow_i} - L_{rod_i} + \frac{1}{2}w_{port_i} \leq s_i - L_{spr_i} + L_{land_i} < -\frac{1}{2}w_{port_i}$
R_1	$-\frac{1}{2}w_{port_i} \leq s_i - L_{spr_i} + L_{land_i} < \frac{1}{2}w_{port_i}$
H_0	$L_{spr_i} + \frac{1}{2}w_{port_i} \leq s_i + L_{land_i} \leq L_{valve_i} - L_{spr_i} - L_{rod_i} - \frac{1}{2}w_{port_i}$
F_1	$\frac{1}{2}w_{port_i} < s_i - L_{valve_i} + L_{spr_i} + L_{rod_i} + L_{land_i} \leq \frac{1}{2}w_{port_i}$
F_0	$L_{valve_i} - L_{spr_i} - L_{rod_i} + \frac{1}{2}w_{port_i} < s_i + L_{land_i} \leq L_{spr_i} + L_{flow_i} - \frac{1}{2}w_{port_i}$
F_{1-}	$-\frac{1}{2}w_{port_i} < s_i - L_{spr_i} - L_{flow_i} + L_{land_i} \leq \frac{1}{2}w_{port_i}$
H_{1-}	$s_i > L_{spr_i} + L_{flow_i} - L_{land_i} + \frac{1}{2}w_{port_i}$

The fluid flow area in the valve and spring chambers depends on the spool displacement. The fluid flow areas for the valve chambers and the spring chambers are given by

$$A_{Cvalve_i} = \begin{cases} A_{port_i}, & \text{for } R_{0,1},\ F_{0,1},\ H_0 \\ \alpha_{11}A_{port_i}, & \text{for } R_{1+} \\ \alpha_{12}A_{port_i}, & \text{for } F_{1-} \\ 0, & \text{otherwise} \end{cases} \tag{31a}$$
$$\alpha_{11} = (s_i + L_{land_i} + L_{rod_i} - L_{spr_i} - L_{flow_i} + 0.5\, w_{port_i})w_{port_i}^{-1}$$
$$\alpha_{12} = \frac{L_{rod_i}}{w_{port_i}} - \alpha_{11} + 1$$
$$A_{Pvalve_i} = \begin{cases} A_{port_i}, & \text{for } F_{1-,0},\ H_{1+} \\ \alpha_2 A_{port_i}, & \text{for } F_1 \\ 0, & \text{otherwise} \end{cases} \tag{31b}$$
$$\alpha_2 = \alpha_{11} - \frac{L_{flow_i}}{w_{port_i}}$$
$$A_{Tvalve_i} = \begin{cases} A_{port_i}, & \text{for } R_{1+,0},\ H_{1-} \\ \alpha_3 A_{port_i}, & \text{for } R_1 \\ 0, & \text{otherwise} \end{cases} \tag{31c}$$
$$\alpha_3 = \left(L_{spr_i} + 0.5w_{port_i} - s_i - L_{land_i}\right) w_{port_i}^{-1}$$
$$A_{Pspr_{li}} = \begin{cases} A_{port_i}, & \text{for } H_{1-} \\ \alpha_4 A_{port_i}, & \text{for } R_{1+} \\ 0, & \text{otherwise} \end{cases} \tag{31d}$$
$$\alpha_4 = \frac{L_{flow_i} - L_{land_i}}{w_{port_i}} - \alpha_{11} + 1$$
$$A_{Tspr_{ri}} = \begin{cases} A_{port_i}, & \text{for } H_{1+} \\ \alpha_5 A_{port_i}, & \text{for } F_{1-} \\ 0, & \text{otherwise} \end{cases} \tag{31e}$$
$$\alpha_5 = \left(s_i + 0.5\, w_{port_i} - L_{spr_i}\right) w_{port_i}^{-1}$$

where A_{Cvalve_i}, A_{Pvalve_i}, and A_{Tvalve_i} are the flow areas for fluid flow from the cylinder port, pump port and tank port, respectively. $A_{Pspr_{li}}$ are the flow areas for flow from the pump

to the left side spring assembly, and $A_{Tspr_{ri}}$ are the flow areas for flow from the right side spring assembly to the tank. The port areas, A_{port_i}, are defined as

$$A_{port_i} = \pi \left(d_{spool_i} + 2\Delta R_i\right) w_{port_i} \tag{32}$$

The fluid flow from one chamber to another depends on these flow areas. For a particular flow path, when the flow area is equal to 0, the valve is closed for that path. On the other hand, when the flow area is equivalent to A_{port}, the valve is fully open. In other scenarios, the valve is partially open or partially closed. If radial clearance is present in the valves, leakage flow exists from the valve chamber towards the spring chambers. For radial clearances of ΔR_i, $(i \in \{dcv_p, dcv_s\}$, the leakage areas are given by

$$A_{leak_i} = \frac{\pi}{4}\left(\left(d_{spool_i} + \Delta R_i\right)^2 - d_{spool_i}^2\right) \tag{33}$$

where d_{spool_i} are the diameter of the spools.

The volume of the ports, valve chamber, and spring chambers are defined as

$$V_{port_i} = \frac{\pi}{4}\left(d_{port_i}^2 - d_{valve_i}^2\right) w_{port_i} \tag{34a}$$

$$V_{valve_i} = \frac{\pi}{4}\left(d_{valve_i}^2 - d_{rod_i}^2\right) L_{rod_i} + \frac{\pi}{2}\left(d_{valve_i}^2 - d_{spool_i}^2\right) L_{land} \tag{34b}$$

$$V_{spr_{ri}} = \frac{\pi}{4}\left(d_{valve_i}^2 - d_{sol_i}^2\right) L_{spr_i} + \max\left(0, \frac{\pi}{4} d_{valve_i}^2 \left(s_i - L_{spr_i}\right)\right) \tag{34c}$$

$$V_{spr_{li}} = \frac{\pi}{4}\left(d_{valve_i}^2 - d_{sol_i}^2\right) L_{spr_i} + \max\left(0, \frac{\pi}{4} d_{valve_i}^2 \left(L_{valve_i} - L_{spr_i} - L_{rod_i} - 2L_{land_i} - s_i\right)\right) \tag{34d}$$

where $d_{valve_i} = d_{spool_i} + 2\Delta R_i$, and d_{sol_i}, L_{rod_i} are the diameters of the solenoid rod and the spool rod, respectively. The hydraulic capacitance for the corresponding fluid pressure (P_k) is determined as $C_{h_k} = \frac{B_{hyd}}{V_k}$. Using the expression for the volumes and the flow equations, the dynamics of fluid pressures in the chambers and ports can be determined from the standard expressions of pressure change and fluid flow in hydraulics.

A detailed model for the solenoid is required for precise and accurate control. The solenoid model in [26] with the nonlinear current dynamics and magnetic force expression is used here.

VIII. POWERTRAIN MODEL

The powertrain consists of

1) an SI engine actuated by a linear actuator,
2) a lockup torque converter actuated with ON-OFF solenoid valves and a hydraulic piston,
3) a double pinion planetary gear set in which the clutches are actuated ON-OFF solenoid valves and hydraulic pistons,
4) a push belt type CVT whose pulley movements are actuated using 3-way 3-position DCVs, and
5) a hydraulic system consisting of a centrifugal gear pump, a pressure relief valve, a pressure reducing valve, valves for actuation of the lockup torque converter, planetary gear set, and the CVT.

We aggregate the models of the torque converter, planetary gearbox, CVT, hydraulic systems, and the engine to develop a model for an ICE powertrain with CVT. For modeling the engine, the control-oriented mean value model [4], [27] is used. A linear actuator with a ball-screw mechanism is used for throttle actuation [28].

The aggregated model is a DAE system consisting of 69 states and 11 inputs. Fig. 1 gives an overview of the states and inputs in each sub-system of the powertrain. One algebraic state is obtained from the algebraic constraint involving the angular velocities of the gears in the planetary gear set. The other is from the algebraic constraint relating the pulley radii and the variator length in the CVT. The powertrain model developed exhibits state-dependent switching triggered by external torque on the gears of the planetary gear set. The choice of the algebraic state in the planetary gear depends on the external gear torque(s), which is(are) dominant over others.

IX. UNIFIED MODEL FOR LONGITUDINAL MOTION

The behaviour of a powertrain can be validated by analyzing the longitudinal motion behaviour of a vehicle only. Here, we combine the proposed powertrain model with a brake model, a tyre model, wheel dynamics, and longitudinal dynamics of a quarter car vehicle model. The longitudinal vehicle dynamics can be expressed as

$$M_v \frac{\mathrm{d}v_x}{\mathrm{d}t} = F_x - R_x - M_v g \sin(\theta_{road}) - F_{aero} \tag{35}$$

where θ_{road} is the slope of the road and F_{aero} is the aerodynamic drag on the vehicle. F_x and R_x are the tractive force and rolling resistance at the tyre road contact, respectively. Since the objective is to showcase the characteristics of the powertrain model, any brake model capturing the transient and steady-state characteristics of the brakes fulfills the objective. The dynamic model of a brake operated by a vacuum booster developed by Gerdes [29] is used here. The wheel dynamics and the Tyre model is described in Section IX-A.

A. TYRE MODEL

A quarter car vehicle model demonstrates an average behaviour of a vehicle. Therefore, only the final reduction ratio is taken for the differential, i.e., it is replaced with a fixed gear ratio, r_d, with efficiency η_d. The wheel rotation can be described by

$$J_w \frac{\mathrm{d}\omega_w}{\mathrm{d}t} = \tau_w - R_w F_x + R_w R_x \tag{36}$$

where $\omega_w = r_d \omega_{cvt_s}$ and $\tau_w = \frac{1}{\eta_d r_d}\tau_d$. Here, J_w, ω_w, τ_w, and R_w are the tyre-wheel inertia, wheel angular velocity

along the wheel x-axis, drive torque from the differential and effective radius of the tyre, respectively. The drive torque at the wheel is related to the load torque at the secondary pulley of the CVT. Hence (36) can be rearranged and substituted in the rotational dynamics of the CVT secondary to obtain a single differential equation.

The Magic formula Tyre model [6] is used to obtain the tractive force. A drawback of the Tyre model in [6] is that the slip definition restricts the usage of the model to accelerating conditions and steady-state velocities only. The slip definition is modified by adding conditions for scenarios where either or both the vehicle's longitudinal velocity and the tyre's angular velocity are zero. The added conditions for slip angle and the Magic formula are given as

$$K_t = \begin{cases} 0, & \text{if } v_x = R_w\omega_w \\ -1, & \text{if } \omega_w = 0 \text{ and } v_x \begin{cases} < 0 & \textit{Drive} \\ > 0 & \textit{Reverse} \end{cases} \\ 1, & \text{if } v_x = 0 \text{ and } \omega_w \begin{cases} < 0 & \textit{Drive} \\ > 0 & \textit{Reverse} \end{cases} \\ \tilde{K}_t, & \text{otherwise} \end{cases}$$

$$\tilde{K}_t = \begin{cases} \dfrac{-v_x + R_w\omega_w}{\max(v_x, R_w\omega_w)}, & \textit{Drive} \\ \dfrac{v_x - R_w\omega_w}{\min(v_x, R_w\omega_w)}, & \textit{Reverse} \end{cases} \tag{37}$$

X. CVT CONTROLLER

Powertrains with CVT comprise a controller that determines a transmission ratio based on vehicle states such as the vehicle's velocity, throttle angle in the engine, etc. The controller provides inputs to the inflow-outflow valves to obtain the desired transmission ratio and alters the hydraulic pressure in the pulley cylinders [30], [31]. As a result, the pulley radii change, and therefore, the transmission ratio. Here, the CVT controller sets the geometric ratio of the CVT, $r_{g_{cvt}}$, for the desired transmission ratio. The desired geometric ratio is taken to be a function of the throttle angle, α_e, and the longitudinal velocity, v_x. The control strategy is contemplated to make the CVT behave like a five-stage automatic transmission such that the powertrain model's behaviour can be compared with the behaviour of other combinations of powertrains with automatic transmissions. Here, the desired geometric ratio ($r_{d_{cvt}}$) values are set to five discrete values. Although CVTs can provide infinite transmission ratios for steady-state operation, in this case, the geometric ratio has only five steady-state values.

It is considered that when the gear mode is *Neutral* or *Reverse*, the desired geometric ratio takes its lowest value of 0.4352, which is the same as the initial value of $r_{g_{cvt}}$. The desired geometric ratio for the $k+1^{\text{th}}$ iteration, $r_{d_{cvt}}[k+1]$, is defined as

$$r_{d_{cvt}}[k+1] = \begin{cases} f_{cvt}\left(\alpha_e[k], v_x[k], \Delta\alpha_e[k]\right) = f_{cvt}[k], \\ \qquad \text{if Gear Mode} \rightarrow \textit{Drive} \\ 0.4352, \quad \text{otherwise} \end{cases} \tag{38}$$

where $\Delta\alpha_e[k] = \alpha_e[k] - \alpha_e[k-1]$, and

$$f_{cvt}[k] = \begin{cases} f_{ds}\left(\alpha_e[k], v_x[k]\right), & \text{if } \Delta\alpha_e[k] < 0 \\ f_{cvt}[k-1], & \text{if } \Delta\alpha_e = 0 \\ f_{us}\left(\alpha_e[k], v_x[k]\right), & \text{if } \Delta\alpha_e[k] > 0 \end{cases}$$

The functions $f_{ds}(\cdot)$ and $f_{us}(\cdot)$ are for downshifting and up-shifting the gear ratios, respectively. The shifting functions are defined in a manner such that the functions depend on longitudinal velocity (v_x), and the throttle angle (γ_e). These functions are defined as

$$f_{shift}[k+1] = \begin{cases} 0.4352, & \text{if } \bar{v}_x[k] \le \Upsilon_1 \\ 0.67, & \text{if } \Upsilon_2 > \bar{v}_x[k] \ge \Upsilon_1 \\ 0.93, & \text{if } \Upsilon_3 > \bar{v}_x[k] \ge \Upsilon_2 \\ 1.215, & \text{if } \Upsilon_4 > \bar{v}_x[k] \ge \Upsilon_3 \\ 1.6639, & \text{if } \bar{v}_x[k] \ge \Upsilon_4 \end{cases} \tag{39}$$

where $\Upsilon_i = \Upsilon_i(\gamma_e[k])$ $(i = 1, 2, 3, 4)$, $\gamma_e[k] = \left\lfloor \frac{10}{9}\alpha_e[k] \right\rfloor + 1$ is the scaled throttle, and $\bar{v}_x = 3.6\, v_x$, i.e., velocity in kilometers per hour. The boundary functions $\Upsilon_i(\cdot)$, $i = 1, 2, 3, 4$, depend on the scaled throttle but are different for the up-shifting and downshifting functions. The boundary functions for the up-shifting are defined as

$$\begin{aligned} \Upsilon_1(x) &= 25u(x) + \frac{5}{4}r(x-50) - \frac{5}{4}r(x-90) \\ \Upsilon_2(x) &= 65u(x) + \frac{7}{4}r(x-40) - \frac{19}{16}r(x-50) \\ &\quad - \frac{9}{16}r(x-90) \\ \Upsilon_3(x) &= 90u(x) + \frac{4}{3}r(x-10) + \frac{1}{6}r(x-40) \\ &\quad - r(x-50) - \frac{1}{2}r(x-90) \\ \Upsilon_4(x) &= 135u(x) + \frac{5}{6}r(x-10) + \frac{7}{6}r(x-40) \\ &\quad - \frac{5}{4}r(x-50) - \frac{3}{4}r(x-90) \end{aligned}$$

where $u(\cdot)$ and $r(\cdot)$ are unit step and ramp functions, respectively. Similarly, the boundary functions for the downshifting are defined as

$$\begin{aligned} \Upsilon_1(x) &= 10u(x) + \frac{1}{10}r(x-10) + \frac{2}{5}r(x-40) \\ &\quad - \frac{3}{25}r(x-50) - \frac{19}{50}r(x-90) \\ \Upsilon_2(x) &= \frac{166}{5}u(x) + \frac{19}{150}r(x-10) + \frac{101}{150}r(x-40) \\ &\quad - \frac{49}{80}r(x-50) - \frac{3}{16}r(x-90) \\ \Upsilon_3(x) &= 50u(x) + \frac{7}{15}r(x-10) + \frac{1}{30}r(x-40) \\ &\quad - \frac{9}{40}r(x-50) - \frac{11}{40}r(x-90) \\ \Upsilon_4(x) &= 70u(x) + \frac{2}{15}r(x-10) + \frac{29}{30}r(x-40) \\ &\quad - \frac{17}{20}r(x-50) - \frac{1}{4}r(x-90) \end{aligned}$$

Here, a simple rule-based controller with boundary constraints is used for achieving the task. The control strategy together with the boundary constraints for the primary direction control valve is elaborated as follows:

$$u_{sol_{pl}} = \begin{cases} E_{sol_{pl}}, & r_{d_{cvt}} < r_{g_{cvt}} \text{ or } P_{p_{cvt}} > P_{p_{ub}} \text{ or} \\ & R_{p_{cvt}} > R_{p_{ub}} \\ 0, & \text{otherwise} \end{cases} \tag{40a}$$

$$u_{sol_{pr}} = \begin{cases} E_{sol_{pr}}, & r_{d_{cvt}} > r_{g_{cvt}} \text{ or } P_{p_{cvt}} < P_{p_{sb}} \text{ or} \\ & R_{p_{cvt}} < R_{p_{sb}} \\ 0, & \text{otherwise} \end{cases} \tag{40b}$$

where the suffixes *ub* and *sb* represent the upper bound and lower bound of the respective states. If both the left and right solenoids have non-zero inputs, i.e., if $u_{sol_{pl}} = u_{sol_{pr}} \neq 0$, then

$$u_{sol_{pl}} = \begin{cases} E_{sol_{pl}}, & R_{p_{cvt}} > R_{p_{ub}} \text{ or } \left(P_{p_{cvt}} > P_{p_{ub}}\right. \\ & \left. \text{and } R_{p_{cvt}} \in \left(R_{p_{sb}}, R_{p_{ub}}\right)\right) \\ 0, & \text{otherwise} \end{cases} \tag{41a}$$

$$u_{sol_{pr}} = \begin{cases} E_{sol_{pr}}, & R_{p_{cvt}} < R_{p_{sb}} \text{ or } \left(P_{p_{cvt}} < P_{p_{sb}}\right. \\ & \left. \text{and } R_{p_{cvt}} \in \left(R_{p_{sb}}, R_{p_{ub}}\right)\right) \\ 0, & \text{otherwise} \end{cases} \tag{41b}$$

Inputs to the secondary directional control valve are given only to keep the hydraulic pressure and the radius of the secondary pulley within the operating bounds, given by

$$u_{sol_{sl}} = \begin{cases} E_{sol_{sl}}, & R_{s_{cvt}} > R_{s_{ub}} \text{ or } \left(P_{s_{cvt}} > P_{s_{ub}}\right. \\ & \left. \text{and } R_{s_{cvt}} \in \left(R_{s_{sb}}, R_{s_{ub}}\right)\right) \\ 0, & \text{otherwise} \end{cases} \tag{42a}$$

$$u_{sol_{sr}} = \begin{cases} E_{sol_{sr}}, & R_{s_{cvt}} < R_{s_{sb}} \text{ or } \left(P_{s_{cvt}} < P_{s_{sb}}\right. \\ & \left. \text{and } R_{s_{cvt}} \in \left(R_{s_{sb}}, R_{s_{ub}}\right)\right) \\ 0, & \text{otherwise} \end{cases} \tag{42b}$$

For ensuring safety, the upper and lower bounds are chosen below the maximum radius and above the minimum radius, respectively. It is considered that the controller achieves the target of obtaining the desired ratio when the following condition is satisfied for the geometric ratio:

$$r_{g_{cvt}} \in [0.99 r_{d_{cvt}}, 1.01 r_{d_{cvt}}]$$

Though directional control valves are explicitly used for controlling the flow of fluids precisely and accurately, here, the direction control valves are provided with 10V and 0V for ON and OFF states only.

XI. SIMULATION SETUP

For simulation studies, parameters of the engine model are taken from [4], and parameters for the torque converter model are taken from [3]. Parameters of models of the CVT and the hydraulic system are taken from [14], [22], [32]. The initial conditions are chosen based on actual scenarios in a vehicle. After the powertrain is initiated, the vehicular systems overcome an initial transient phase and settle down, and the vehicle becomes ready for longitudinal motion. Thus, a time gap is considered, after which the gear mode is changed from *Neutral* to the desired gear mode. In all the case study examples in Section XII, a time-gap of 5 seconds is used. A small positive value is taken for the engine's initial angular velocity, assuming an electric motor kick-starts the engine as the ignition turns ON. The initial conditions for the simulation studies are tabulated in Table 3.

All the actuators used in the powertrain model, i.e., the linear actuator of the engine, solenoid valves in the clutches, and directional control valves in the CVT, are usually operated using pulse width modulation (PWM) signals. In this paper, the inputs to all the actuators are considered direct current (DC) voltages that can easily be extended to PWM inputs. Input to the engine actuator varies between 0-12V. While the engine is idle, the actuator's input is 2V. Otherwise, the minimum voltage to the engine is 2.5V. 5V input is given to the engine actuator as the starting voltage. 5V DC input is given to the solenoid valves when turned ON, and 0V DC input is given when they are OFF. All the inputs are updated at intervals of 0.1 seconds. It is assumed that all the states are system outputs, i.e., the system is completely observable.

The clutches are considered to be fully engaged after the clutch disks overcome the stick-slip behaviour and the absolute difference between the angular velocities of the clutches and the attaching component (impeller for the torque converter clutch and ring gear for the forward and reverse clutch) is below 10^{-8}. However, to ensure the clutches are engaged only when difference remains below 10^{-8}, the clutches are engaged after observing the difference to be below 10^{-8} for multiple iterations of the ODE solver. The clutch engagement strategy is given by

$$\text{clutch} \longrightarrow \begin{cases} \text{engaged}, & |\omega_{clutch} - \omega_{ac}| < 10^{-8} \\ & \text{and } N > 200 \\ \text{disengaged}, & \text{otherwise} \end{cases}$$

where ω_{clutch} and ω_{ac} are the angular velocities of the clutches and the attaching components, respectively, and N is the number of iterations of the ODE solver within a sampling interval.

XII. CASE STUDIES

We now present case studies to demonstrate the characteristics of the powertrain model under different operating conditions. The examples show the powertrain's behaviour during a change in gear mode, increase and decrease in transmission ratio, engine idling, torque converter locking-unlocking in different realistic scenarios such as a vehicle accelerating and decelerating in traffic, stop and go at a traffic signal and reverse motion. To be specific, the case studies illuminate the following features:

(a) engine and torque converter responses during gear shifts in *Drive* mode,
(b) torque converter locking and unlocking,

TABLE 3. Initial conditions for some of the powertrain states.

Variable	Symbol	Initial Condition
Armature current in the engine's linear actuator	i_{em}	0 A
Linear actuator motor shaft's angular displacement	θ_{em}	0 rad
Linear actuator motor shaft's angular velocity	ω_{em}	0 rad/s
Intake manifold pressure	P_e	1.1×10^5 Pa
Angular velocity of engine shaft	ω_e	0.01 rad/s
Angular displacement of torque converter impeller stator, turbine and torque converter clutch	$\theta_i, \theta_s, \theta_t, \theta_{tcc}$	0 rad
Angular velocity of torque converter stator, turbine and torque converter clutch	$\omega_s, \omega_t, \omega_{tcc}$	0 rad/s
Relative fluid velocity in the torque converter	v_{tc}	0 m/s
Angular displacements of forward and reverse clutch	θ_{fc}, θ_{rc}	0 rad
Angular velocity of the forward and reverse clutch	ω_{fc}, ω_{rc}	0 rad/s
Displacement of pistons in forward, reverse and torque converter clutch assemblies	$s_{fcp}, s_{rcp}, s_{tcp}$	0 mm
Velocity of pistons in forward, reverse and torque converter clutch assemblies	$v_{fcp}, v_{rcp}, v_{tcp}$	0 mm/s
Pressure in the forward, reverse and torque converter clutch assemblies	$P_{fcp}, P_{rcp}, P_{tcp}$	10^5 Pa
Angular velocity of planetary ring gear and carrier	ω_{rg}, ω_c	0 rad/s
Geometric ratio of the CVT	$r_{g_{cvt}}$	0.4352
Radius of the CVT primary	$R_{p_{cvt}}$	36.23 mm
Angular velocity of the CVT secondary	ω_{cvt_s}	0 rad/s
Hydraulic pressure in the primary pulley cylinder	P_{cyl_p}	2.64 MPa
Hydraulic pressure in the secondary pulley cylinder	P_{cyl_s}	3.0 MPa
Displacement of the DCV spools	s_{dcv_p}, s_{dcv_s}	23.5 mm
Velocity of the DCV spools	v_{dcv_p}, v_{dcv_s}	0 mm/s
Current in primary DCV solenoids	$i_{dcv_{p1}}, i_{dcv_{p2}}$	0 A
Current in secondary DCV solenoids	$i_{dcv_{s1}}, i_{dcv_{s2}}$	0 A
Hydraulic pressure at the pump head	P_{pump}	10^5 Pa
Displacement of the clutch solenoids	s_{sol_i} [1]	0 mm
Current in the clutch solenoids	i_{sol_i} [1]	0 A

[1] i denotes the inflow and outflow solenoids associated with the clutches

(c) changes in the CVT ratio, radii, and angular velocities during gear shifts,

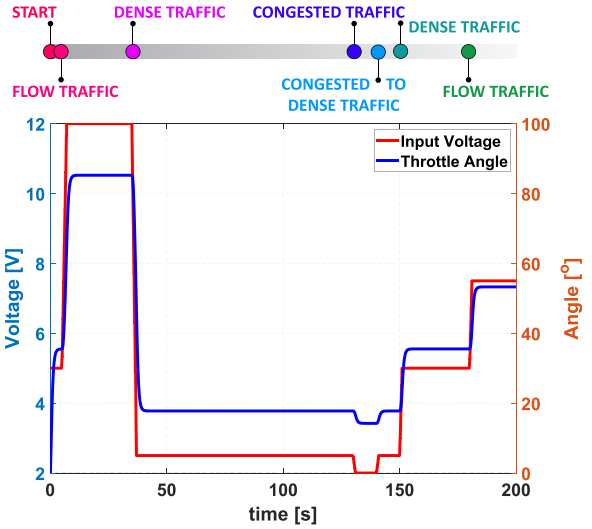

FIGURE 4. The input to the engine actuator and the throttle angle of the engine.

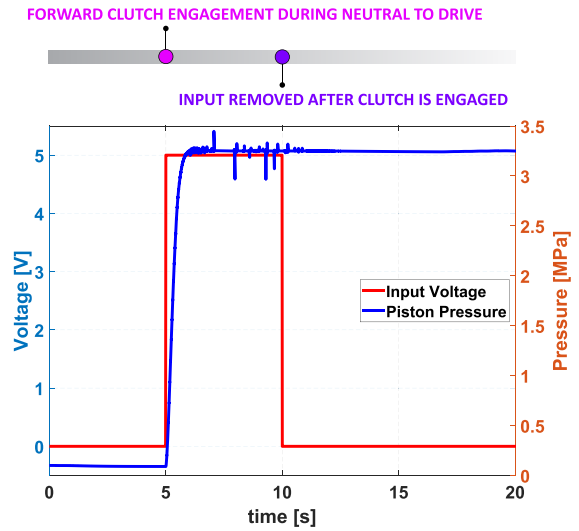

FIGURE 5. The input to the forward clutch inflow solenoid and the hydraulic pressure in the forward clutch assembly.

(d) engine idling,
(e) engine's and torque converter's behaviour during braking, and
(f) continuity of the planetary gears' angular velocities during gear mode interchanges

A. MANEUVERING THROUGH TRAFFIC

This case study example showcases maneuvering of a vehicle in (i) *flow traffic*, (ii) *dense traffic*, and (iii) *congested traffic*. In this example,

(a) the torque converter locking and unlocking,
(b) the engine's and torque converter's behaviour during gear shifts and mild braking,
(c) the CVT behaviour during gear shifts, and

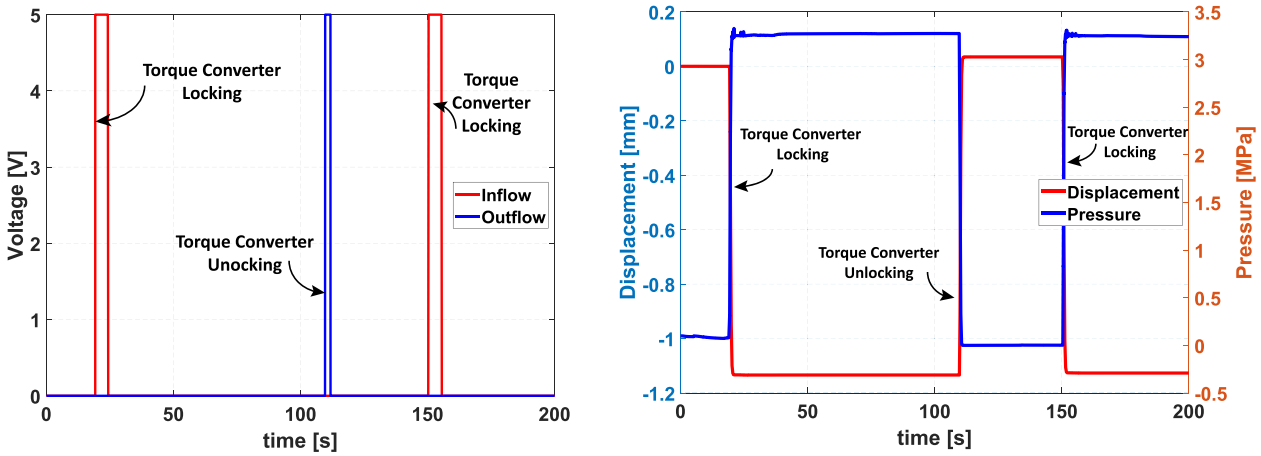

FIGURE 6. (a) The figure on the left shows the inputs to the torque converter clutch's inflow and outflow solenoid valves. (b) The figure on the right shows the piston displacement and hydraulic pressure in the torque converter clutch assembly.

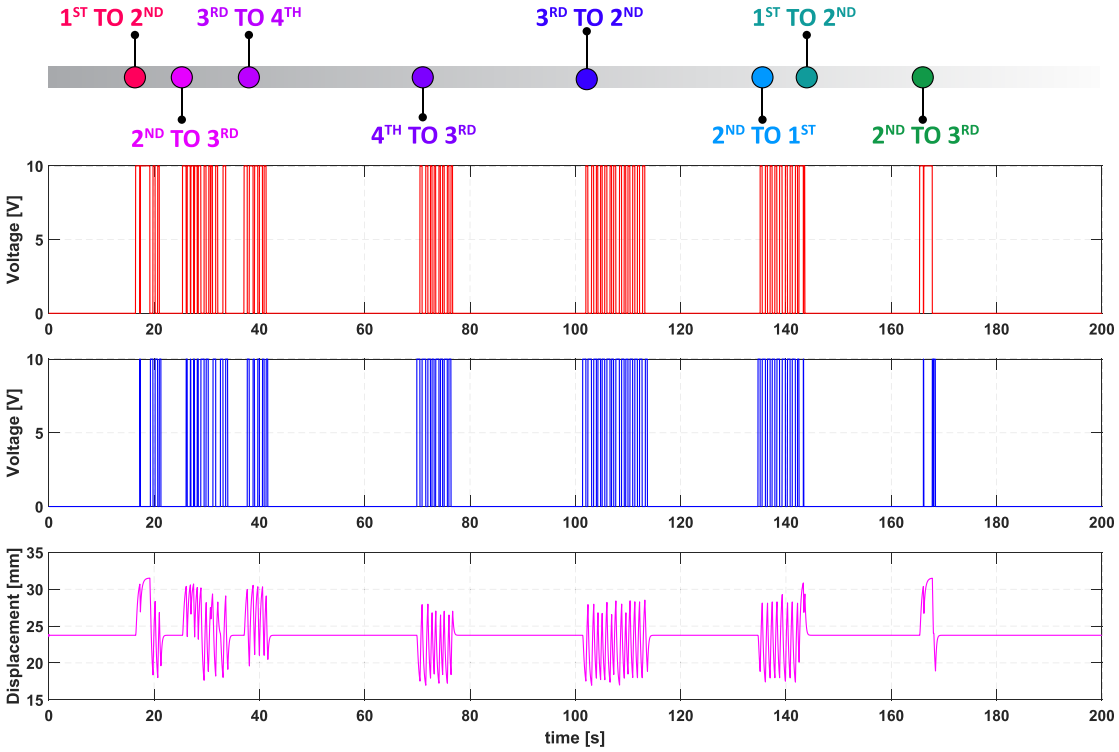

FIGURE 7. The topmost plot shows the input voltage provided to the left solenoid of the primary DCV, the middle plot shows the input voltage provided to the right solenoid of the primary DCV and the lowermost plot shows the spool displacement in the primary DCV.

(d) the planetary gears' continuity w.r.t its angular velocities during *Neutral* to *Drive* are illustrated considering the traffic scenarios.

1) INPUTS

The vehicle starts from rest and begins its motion in a flow traffic scenario, and the engine input is gradually increased until the desired speed is attained. Later as the vehicle encounters a road stretch with dense traffic, the engine input is steadily reduced to maintain the space (or time) headway. Further, as the vehicle enters a congested traffic zone, the engine actuator input is set to idle input voltage, and brakes are applied to slow down to the space (or time) mean speed. Subsequently, as the traffic improves from congested to dense and flow traffic, the throttle increases, and the vehicle speeds up. The input to the engine actuator and the corresponding throttle angle are shown in Fig. 4.

The input to the inflow solenoid in the forward clutch assembly and the resulting piston pressure is shown in Fig. 5. Until 2.5 seconds after the forward clutch is engaged,

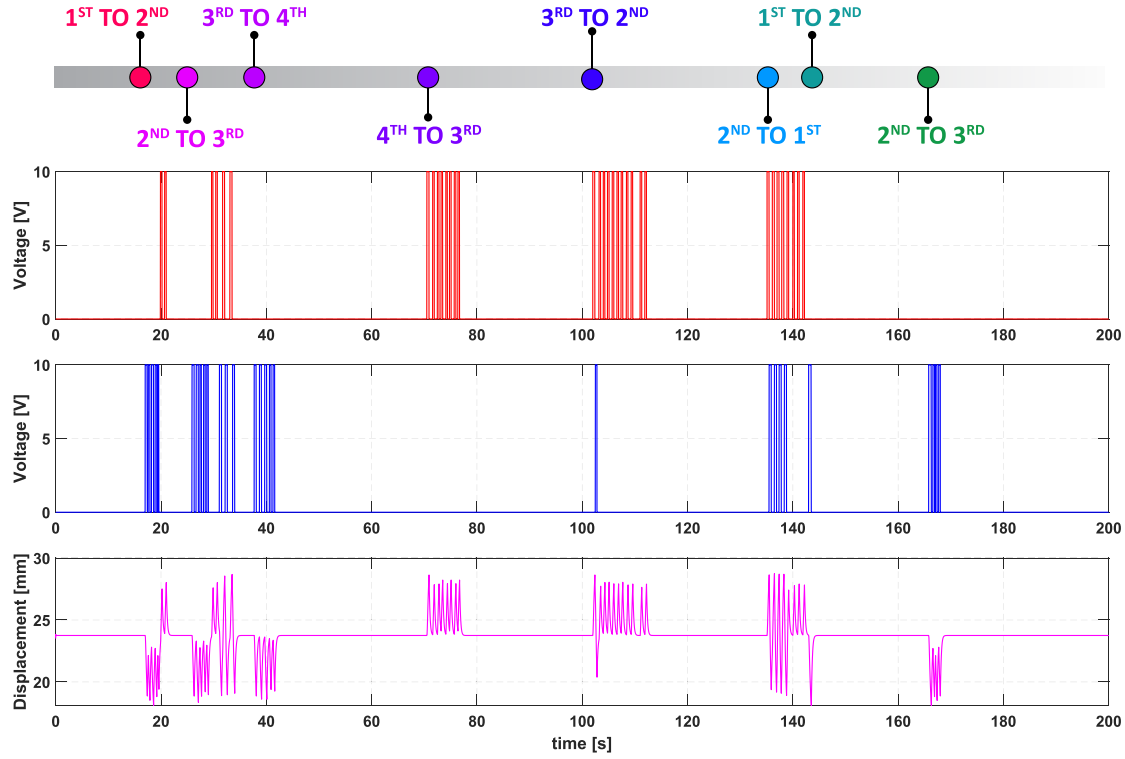

FIGURE 8. The topmost plot shows the input voltage provided to the left solenoid of the secondary DCV, the middle plot shows the input voltage provided to the right solenoid of the secondary DCV and the lowermost plot shows the spool displacement in the secondary DCV.

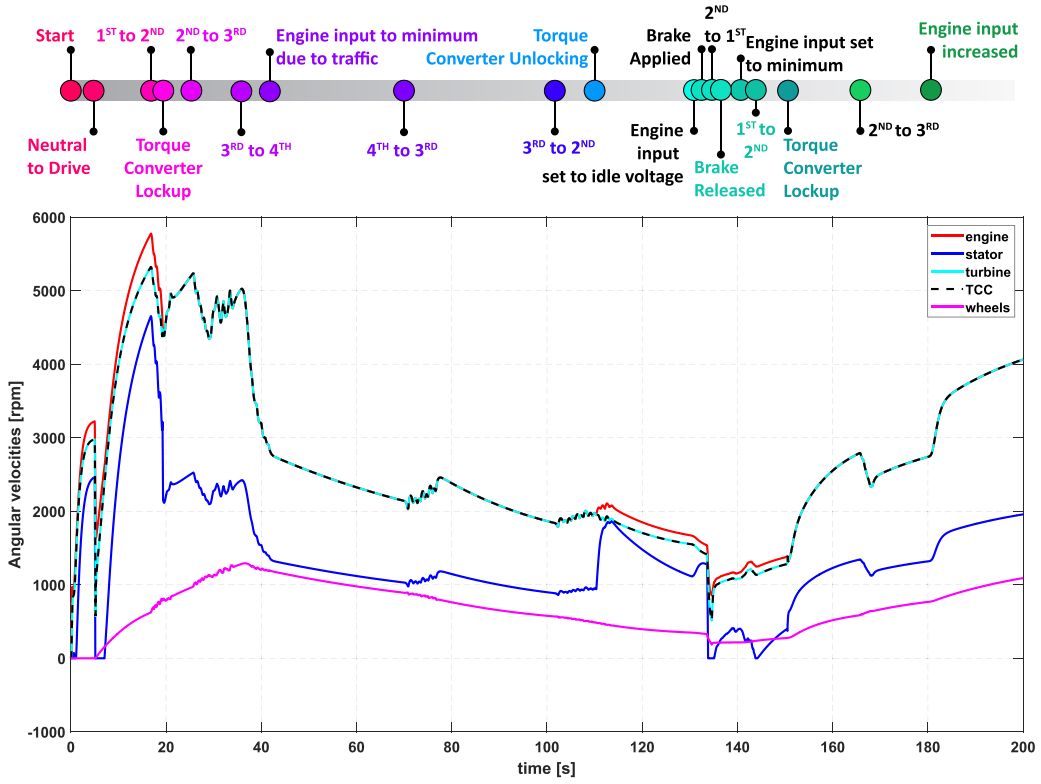

FIGURE 9. Angular velocities of the engine, turbine, stator, torque converter clutch (TCC) and the wheel.

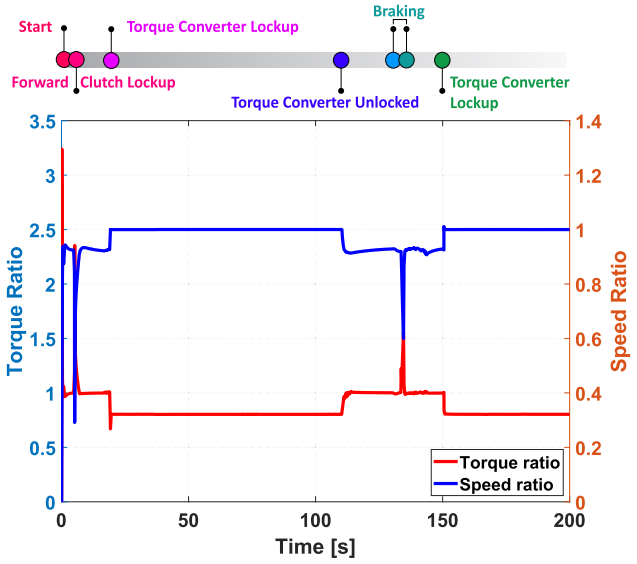

FIGURE 10. Ratios in the torque converter.

no input is given to the torque converter clutch's (TCC) inflow solenoid to let any vibration die out that originated during the clutch engagement. Let the time instant after 2.5 seconds from the forward clutch engagement be t_{pad}. When the torque converter is locked, or the gear mode is changed to *Neutral*, t_{pad} is reset to 0. Also, the torque converter may revert to its previous stage after it gets locked (or unlocked) due to perturbations in the TCC piston pressure. To restrict any fallback, the inflow solenoid and outflow solenoid are given non-zero inputs for time intervals longer than the necessary, denoted by $t_{on|tcc}$ and $t_{off|tcc}$, respectively. The $t_{on|tcc}$ and $t_{off|tcc}$ values are chosen as 5 seconds and 1.5 seconds, respectively. The torque converter clutch's control strategy is given by

$$E_{tcc_{in}} = \begin{cases} 5, & \text{TCC} \to 0 \text{ and } r_{g_{cvt}} > 0.65 \text{ and } t > t_{pad} \\ & \text{and } u_{brake} = 0 \text{ and } u_{eng} > 3.5 \\ 5, & \text{TCC} \to 1 \text{ and } t < t_{on|tcc} \text{ and} \\ & u_{brake} = 0 \text{ and } u_{eng} > 3.5 \\ 0, & otherwise \end{cases}$$

$$E_{tcc_{out}} = \begin{cases} 5, & \text{TCC} \to 1 \text{ and } \big(\text{G.M.} \neq Drive \text{ or } r_{g_{cvt}} \\ & < 0.65 \text{ or } u_{eng} < 3.5 \text{ or } u_{brake} \neq 0\big) \\ 5, & \text{TCC} \to 0 \text{ and } t < t_{off|tcc} \\ 0, & otherwise \end{cases}$$

where TCC values 1 and 0 indicate that the torque converter clutch is locked and unlocked, respectively. The input voltage applied to the torque converter is shown in Fig. 6a, and the subsequent hydraulic pressure and displacement changes in the clutch piston chamber are shown in Fig. 6b.

Like the torque converter, the CVT controller is let to function after a time gap post forward clutch engagement. The input voltages to the primary and secondary DCVs determined by the CVT controller and the resulting spool displacements are shown in Fig. 7 and 8, respectively. In the figure, the abbreviations $1^{st}, 2^{nd}, \cdots, 5^{th}$ resemble the discrete values considered for the upshifting and downshifting function in (39) in ascending order.

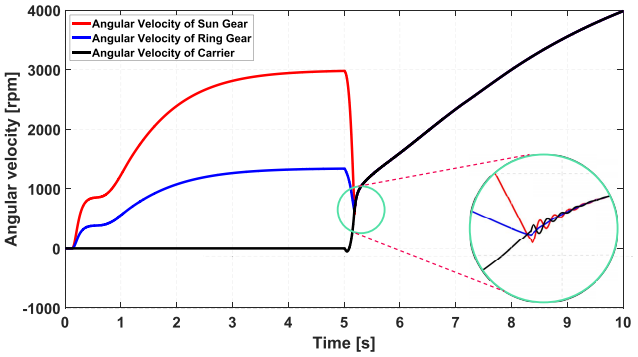

FIGURE 11. Angular velocities of the planetary gear system (up to 10 seconds).

2) BEHAVIOUR OF THE ENGINE AND THE TORQUE CONVERTER DURING GEAR SHIFTS AND MILD BRAKING

The engine crankshaft's angular velocity is expected to experience a stiff decrease due to a sudden increase in load during every upshift of the transmission ratio. Once the steady-state is reached, the angular velocity increases again. The opposite behaviour is expected during transmission downshifting. The expected behaviour is obtained, as can be observed from the angular velocity of the engine crankshaft shown in Fig. 9.

The stator is expected to enhance torque multiplication whenever the torque converter is not steady. Fig. 9 shows the stator stops rotating whenever there is torque demand from the drivetrain, and the torque converter is not locked, such as during shifting in gear mode from *Neutral* to *Drive* and braking.

Whenever brakes are applied, the engine and the torque converter have to overcome an excess load torque, and their angular velocities suffer a rapid decrease from their current values. The same can be observed from the angular velocities of the engine and the torque converter shown in Fig. 9.

3) TORQUE CONVERTER LOCKING AND UNLOCKING

The torque converter clutch gets engaged at around 20 seconds, as shown in Fig. 9, following the control strategy in Section XII-A1 and shown in Fig. 6a. The torque converter clutch is expected to disengage when the vehicle slows down, and the CVT controller brings the transmission ratio below 0.65. The torque converter unlocks at around 115 seconds, meeting the expected response, shown in Fig. 9.

It is expected that when the torque converter is not locked and is in its steady-state, the torque ratio should become one, and the speed ratio should be near one due to loss in the torque converter. Also, when the turbine experiences an instantaneous torque demand during gear mode change and braking, the torque ratio of the torque converter shoots

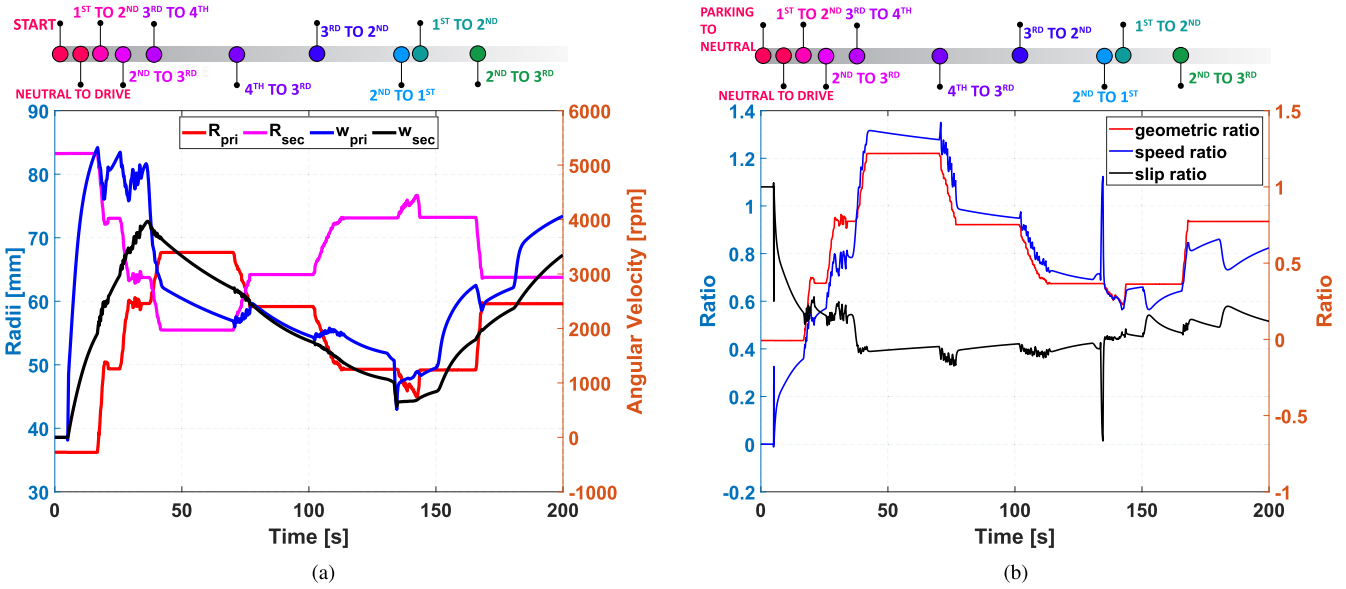

FIGURE 12. (a) The figure on the left shows the radii and angular velocities of the CVT pulleys. The figure on the right shows the geometric, speed and slip ratio of the CVT pulleys.

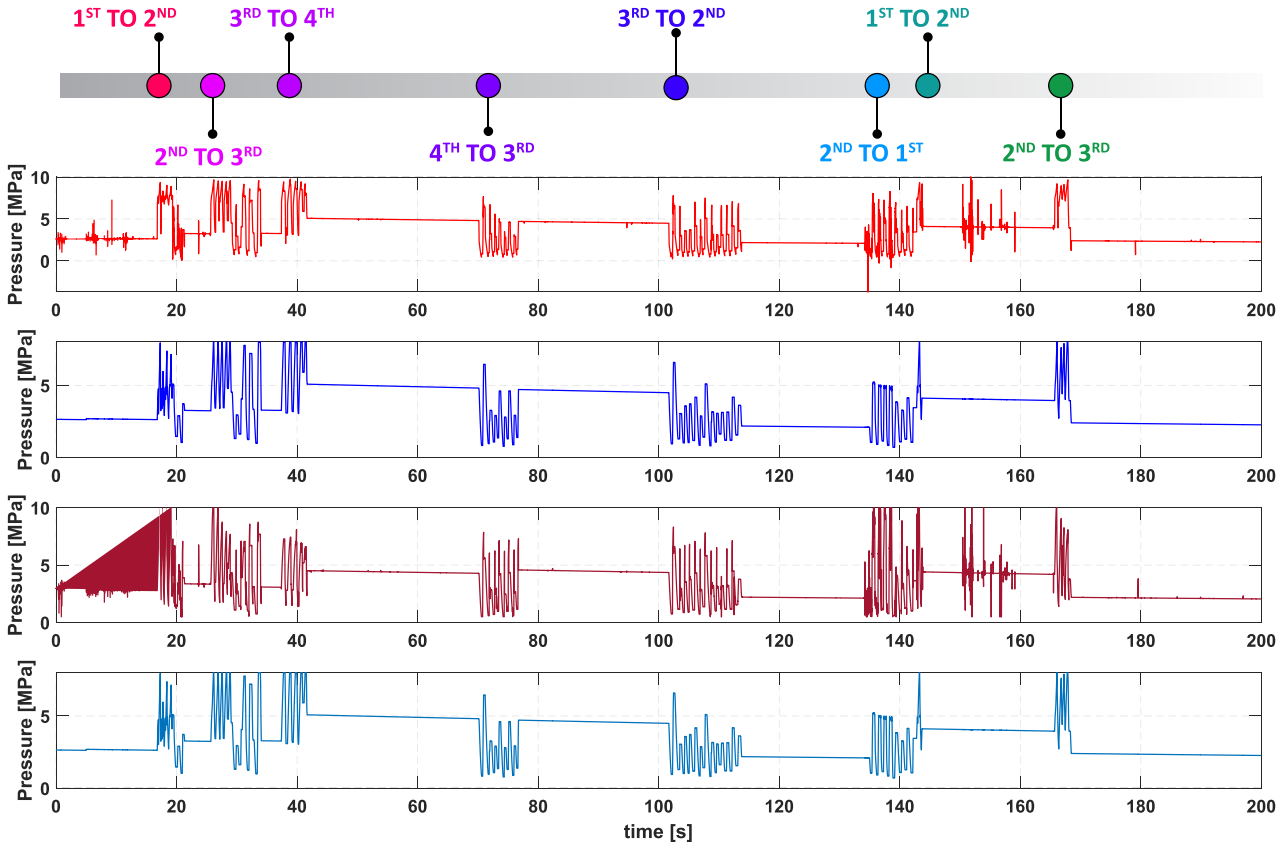

FIGURE 13. The topmost plot shows the valve pressure of the primary DCV. The second plot shows the hydraulic pressure in the primary pulley cylinder. The third plot shows the valve pressure of the secondary DCV, and the bottommost plot shows the hydraulic pressure in the secondary pulley cylinder.

up while the speed ratio dips down. The torque and speed ratio plots in Fig. 10 show that the response is the same as expected.

4) CONTINUITY OF THE PLANETARY GEAR RATIOS

Since the gear ratios are inversely related to their angular velocities, ensuring the latter's continuity is sufficient.

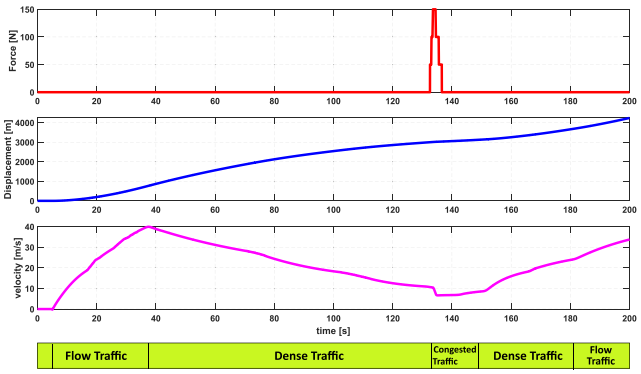

FIGURE 14. The topmost plot shows the input braking force, the middle plot shows the longitudinal displacement of the vehicle, and the lowermost plot shows the longitudinal velocity of the vehicle.

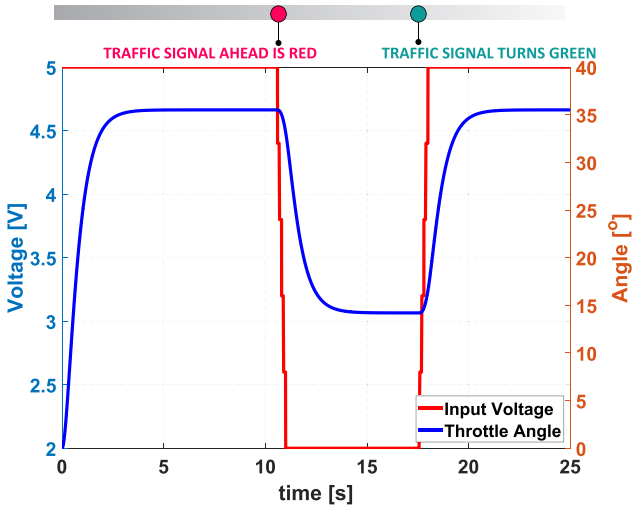

FIGURE 15. The input to the engine actuator and the throttle angle of the engine.

Continuous gear angular velocities can be obtained by incorporating the clutch dynamics and modeling the mechanism of the planetary gears as a DAE. However, it is not sufficient since the constraints on the algebraic state require switching and the dynamics during a change in gear mode.

The continuity in the angular velocities of the planetary gears is shown in Fig. 11. It can be seen that, as the forward clutch starts engaging, the carrier-primary pulley starts rotating, initially in the reverse direction and gradually in the forward direction. Eventually, all the planetary gears attain equal angular velocity, reaching a steady state. The sinusoidal behaviour while approaching steady-state is due to the stick-slip behaviour of the clutch plates. The plots show how *Direct Drive* with gear ratio one is obtained as it should occur.

5) CVT BEHAVIOUR

During transmission upshift, the primary pulley radius increases while that of the secondary decreases. The inverse happens during transmission downshift. Moreover, due to discrete steady-state values of the up and downshifting

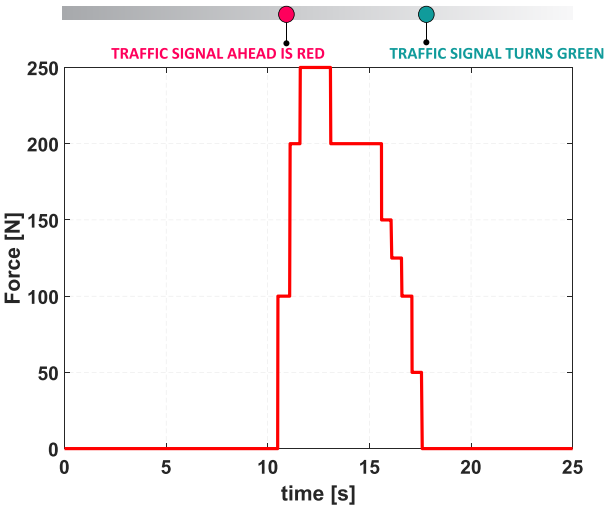

FIGURE 16. The applied braking force.

functions, the radii are expected to attain steady-state values when the geometric ratio reaches steady-state. Plots of the radii and the angular velocities of the CVT pulleys, depicted in Fig. 12a, illustrate that the response is consistent with the expected outcome. The angular velocity of the secondary pulley does not encounter the transitions during gear shifts contrary to that of the primary, which exhibits the expected smooth gear shifting feature of a CVT.

The geometric ratio and the speed ratio vary when the DCV inputs are altered and reach discrete steady-state values given in (39) when the condition in (42) is met. Additionally, the speed ratio experiences stiff variations during gear mode changes, braking, and when the tyres start rolling from rest. The exact behaviour can be observed in Fig. 12b. The variation of the geometric ratio also highlights the efficacy of the rule-based CVT controller in obtaining the desired gear ratio. Also, as shown in the figure, the difference in the CVT's geometric and speed ratio develops a non-zero slip ratio essential for torque transfer from the primary to the secondary.

6) PRESSURE IN DCV CHAMBERS AND PULLEY CYLINDERS

The hydraulic pressures in the DCVs and the pulley cylinders are shown in Fig. 13. The figure indicates the DCVs' valve pressures and the pressures in the pulley cylinders vary when the DCV inputs change, as expected. It can be noticed that contrary to the cylinder pressures, the DCVs' valve pressure suffers few stiff perturbations even when the DCV inputs are 0. These perturbations are due to pressure variations in the pump line, which die out in the cylinders due to damping of the ATF.

7) LONGITUDINAL CHARACTERISTICS OF THE VEHICLE

The braking force, longitudinal displacement and velocity of the vehicle are shown in Fig. 14. The longitudinal displacement and the longitudinal velocity resemble a vehicle's usual behaviour experiencing flow traffic, dense

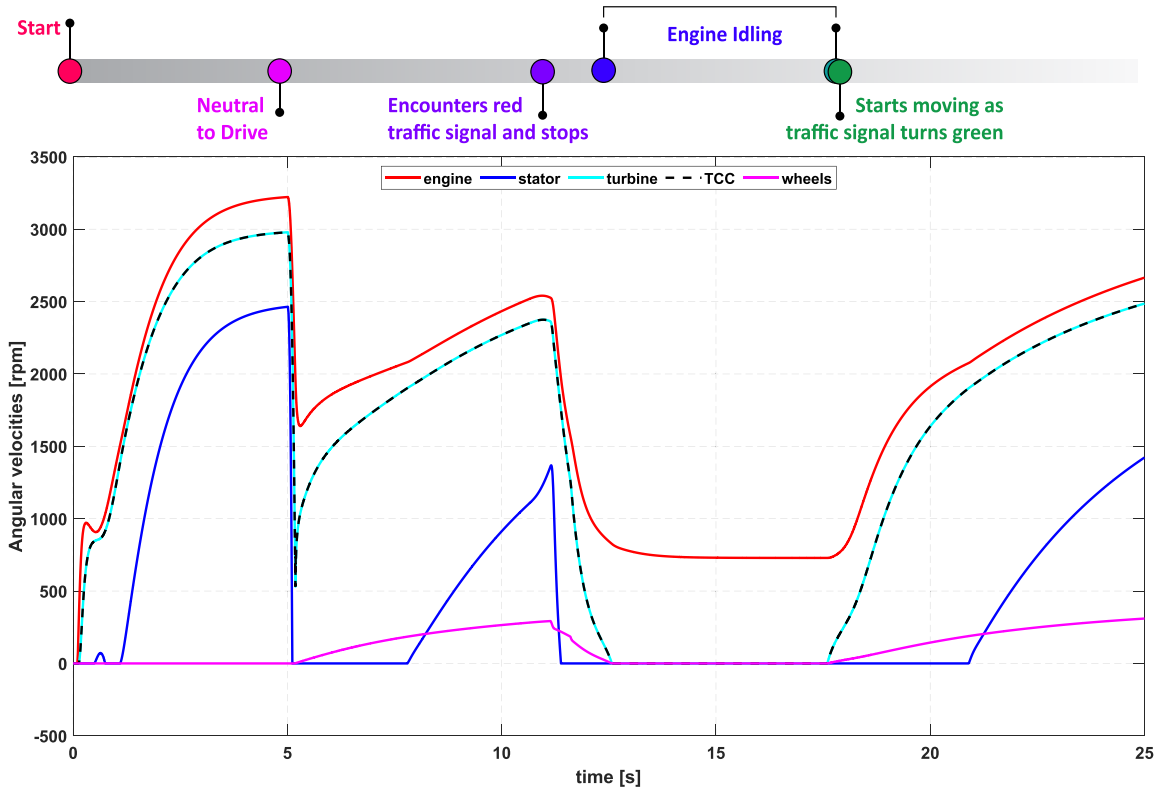

FIGURE 17. Angular velocities of the engine, turbine, stator, torque converter clutch and the wheel.

traffic, and congested traffic. On the congested stretch, brakes are applied, and the engine idles. Therefore the vehicle decelerates and moves at the space (or time) mean speed until it overcomes the congested stretch, after which it accelerates upon encountering dense traffic followed by flow traffic. This longitudinal behaviour ascertains the powertrain model for obtaining and predicting vehicles' motion in traffic scenarios.

To visualize these features better, we developed an animated representation which can be found in doi.org/10.6084/m9.figshare.17950733

B. STOP AND GO

This case study example demonstrates the scenario where a vehicle stops and goes again, for instance, in a traffic signal or at an intersection. The powertrain model's behaviour considering a traffic signal is studied here. The case study aims are to show the following:

(a) Idle start and stop feature, and
(b) ability to fulfill the *Stop and Go* behaviour of a vehicle with the proposed model.

1) INPUTS

The vehicle starts from rest and encounters a red traffic signal after a while. The vehicle comes to rest by applying brakes and reducing the engine actuator input to its idling input. When the traffic signal turns green, the braking force is decreased gradually. After the braking input is removed, the engine actuator input is progressively increased, and the vehicle speeds up. The engine actuator input, the corresponding throttle angle, and the applied braking force are shown in Fig. 15 and Fig. 16, respectively.

For this case study, the gear ratio is kept fixed at 0.4352. Therefore, no inputs are applied to the DCVs. The forward clutch and the TCC are engaged following the same input strategy mentioned in Section XII-A.

2) ENGINE IDLING

When the brakes stop the tyres from rotating, the CVT pulleys, planetary gears, and the turbine also stop rotating. The torque converter isolates the engine, and the engine continues to operate at its idle speed. This engine feature is traditionally known as the Idle Start and Stop (ISS). This feature is obtained with the proposed model in this scenario, as depicted in Fig. 17.

The engine starts idling from around 12.5 seconds until the braking force diminishes at approximately 17.5 seconds. Though no power is transmitted from the engine to the wheels, brakes are applied to prevent any unwanted movement of the vehicle, as shown in Fig. 18.

Upon applying brakes, the torque demand increases at the turbine, and therefore, torque multiplication and speed ratio reduction occur at the torque converter. During the *ISS* behaviour, the hydrodynamic force inside the torque converter is maximum which impacts the turbine blades

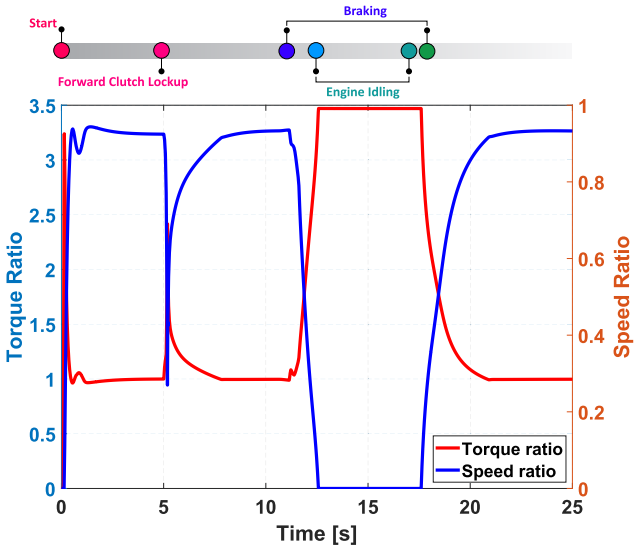

FIGURE 18. Torque ratio and speed ratio of the torque converter.

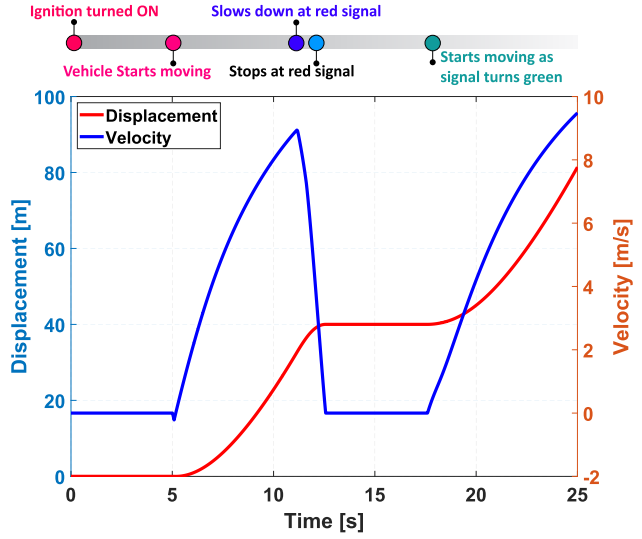

FIGURE 19. Longitudinal displacement and longitudinal velocity of the vehicle.

to rotate. Still, the turbine remains stationary owing to the braking force. Hence, the torque ratio is maximum during this period. This behaviour is obtained in this case study, as shown in Fig. 18.

3) LONGITUDINAL MOTION CHARACTERISTICS

Fig. 19 shows that the vehicle's longitudinal displacement and velocity exactly match the expected outcome in a *Stop-and-Go* scenario. The displacement and velocity curves show that the vehicle slows down and stops at around 12.5 seconds and starts moving again at approximately 17.5 seconds.

To visualize these features better, we developed an animated representation which can be found in doi.org/10.6084/m9.figshare.17950478.

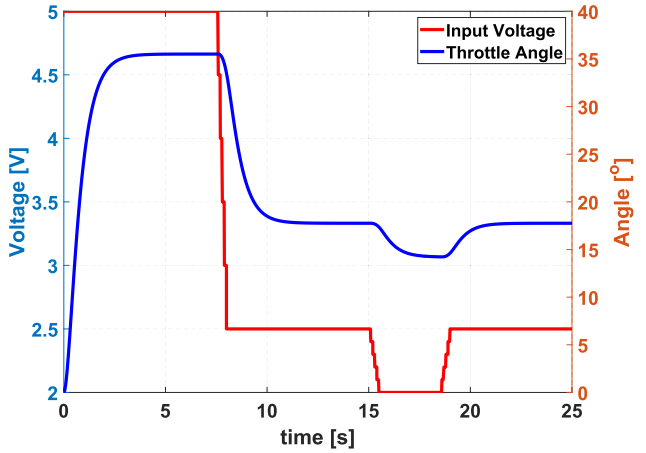

FIGURE 20. The input to the engine actuator and the throttle angle of the engine.

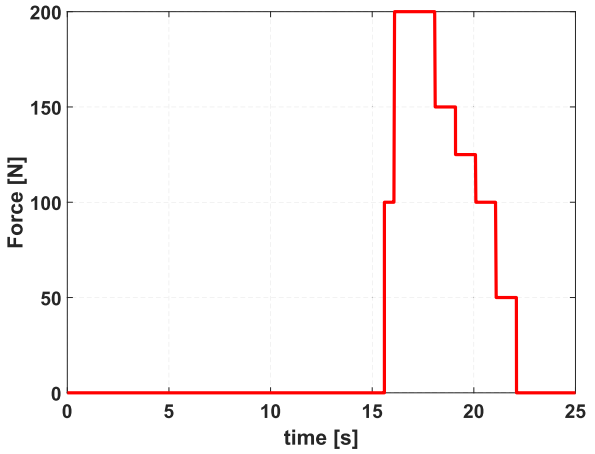

FIGURE 21. The applied braking force.

C. REVERSE MOTION

This case study example illustrates a scenario of perpendicular parking where the vehicle is parked longitudinally in the reverse direction. The vehicle starts from rest, moves to the parking space in the reverse direction, and stops. This case study aims to show

(a) the reverse operation of the proposed powertrain model, and
(b) continuity of the planetary gears' ratios during *Neutral* to *Reverse* and vice-versa.

1) INPUTS

The gear ratio for the reverse operation is chosen as the lowest value of $f_{up/downshift}$ in (39), i.e., 0.4352. In reverse operation, the ratio of the angular velocity of the carrier and the sun gear is

$$\frac{r_{sg}}{r_{rg} - r_{sg}} = r_{rev} \text{ (say)}.$$

Therefore, the overall gear ratio in the reverse operation becomes $\frac{272}{675} r_{rev}$. For maintaining a constant transmission ratio, zero inputs are given to the DCVs.

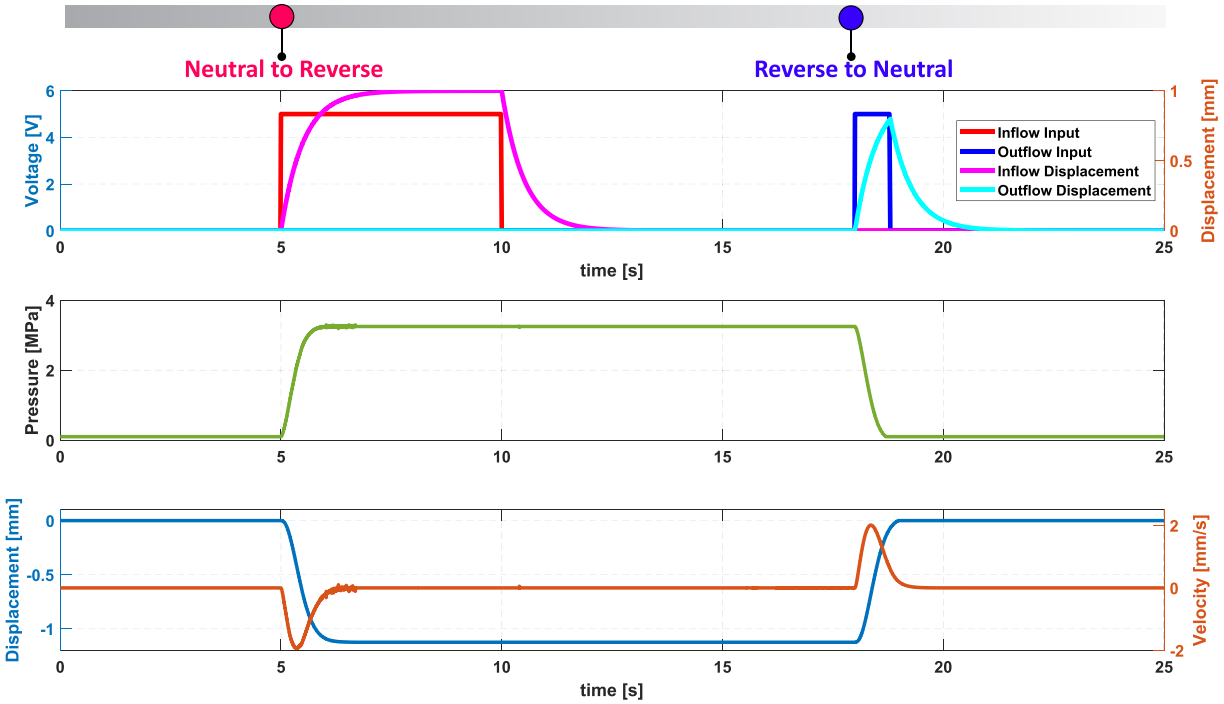

FIGURE 22. The topmost plot shows the input voltages to the inflow and outflow solenoids for the reverse clutch and the displacements of the solenoids, the middle plot shows the hydraulic pressure change in the reverse clutch assembly, and the bottom plot shows the displacement and velocity of the reverse clutch piston.

The input to the engine actuator is its starting voltage from the initial time to the gear mode shift from *Neutral* to *Reverse*. Then it is decreased gradually and kept constant to move the vehicle backward at a low speed. After the vehicle is in the parking position, brakes are applied to stop the vehicle, upon which the engine actuator input is reduced to its idling voltage. Once the vehicle comes to rest, the braking input is withdrawn, the gear mode is changed from *Reverse* to *Neutral*, and the engine actuator's input is increased. Usually, the engine input is kept to its idling voltage once a vehicle is parked. Here, the engine input is increased after the gear mode is changed from *Reverse* to *Neutral* to verify that the car is successfully parked. The applied voltage to the engine actuator and the applied braking force are shown in Fig. 20 and 21, respectively.

The input strategy for the inflow solenoid of the reverse clutch is the same as that of the forward clutch described in Section XII-A. Inputs to the inflow and outflow solenoid valves of the reverse clutch, hydraulic pressure in the clutch assembly, and the displacement and velocity of the clutch piston are shown in Fig. 22. The input to the outflow solenoid is kept non-zero until the gear mode shifts from *Reverse* to *Neutral*.

2) RESPONSE OF POWERTRAIN COMPONENTS

With the inputs mentioned in Section XII-C1, the angular velocities of the engine crankshaft and the torque converter's turbine are expected to rise until the *Neutral* to *Reverse* gear shift and then decrease. Further, when the brakes are applied to stop the vehicle, the turbine is expected to stop rotating entirely, and the engine should enter its idle mode. The wheels (and the CVT pulleys) will rotate in the reverse direction when the reverse clutch starts engaging until the braking torque stops them. Fig. 23 illustrates the angular velocities of the engine, the turbine, and stator of the torque converter, the torque converter clutch.

The plots show all the powertrain components exhibit the expected behaviour for a vehicle in *Reverse* gear. The reverse clutch is safely disengaged since no power is passed to the drivetrain. After the reverse clutch disengages, the gear mode reverts to *Neutral*, and the torque converter starts transmitting torque from the engine to the turbine.

The torque ratio and speed ratio of the torque converter in this case study is expected to be similar to Section XII-B. The same can be observed in Fig. 24.

3) CONTINUITY OF THE PLANETARY GEAR RATIOS

Ensuring continuity of the planetary gears' angular velocities is equivalent to ensuring the continuity of the planetary gear ratios, which is justified in Section XII-A4. Similar to the case of *Neutral* to *Drive*, the algebraic state is switched from the ring gear's angular velocity to that of the carrier's because, in the *Reverse* mode, the ring gear is restricted to rotate by the external torque from the reverse clutch. Fig. 25 depicts the angular velocities of the planetary gears and their continuous

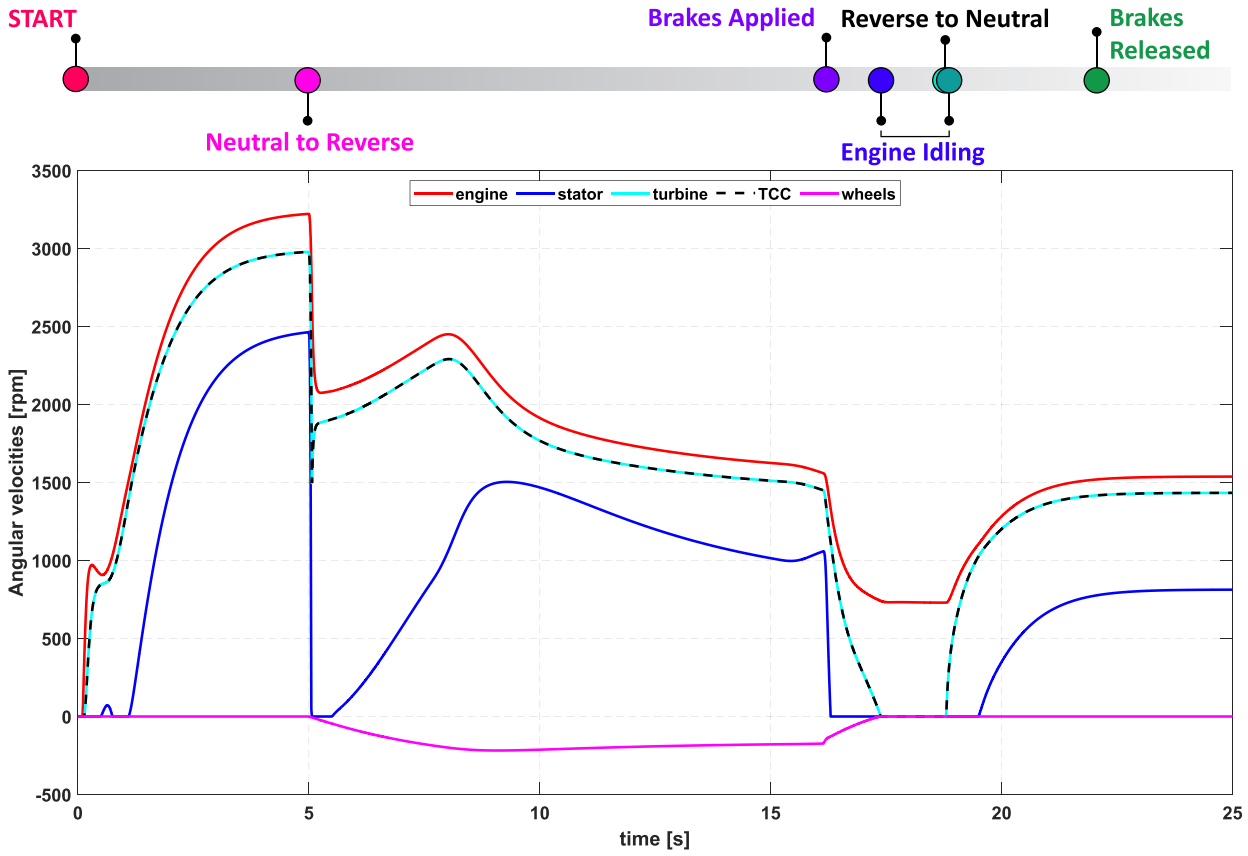

FIGURE 23. Angular velocities of the engine, turbine, stator, torque converter clutch and the wheel.

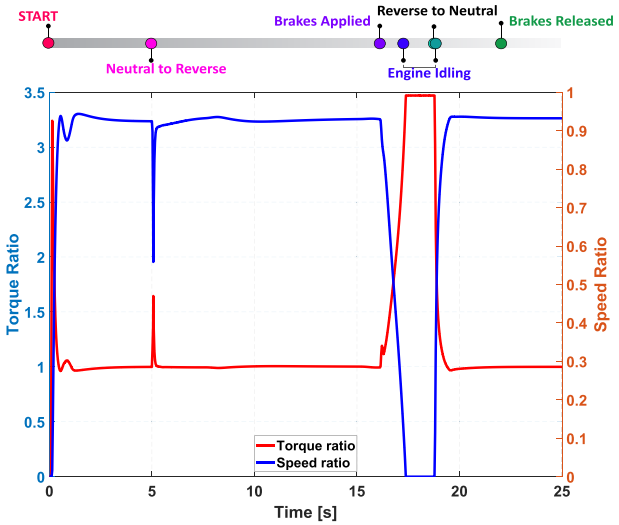

FIGURE 24. Torque ratio and speed ratio in the torque converter.

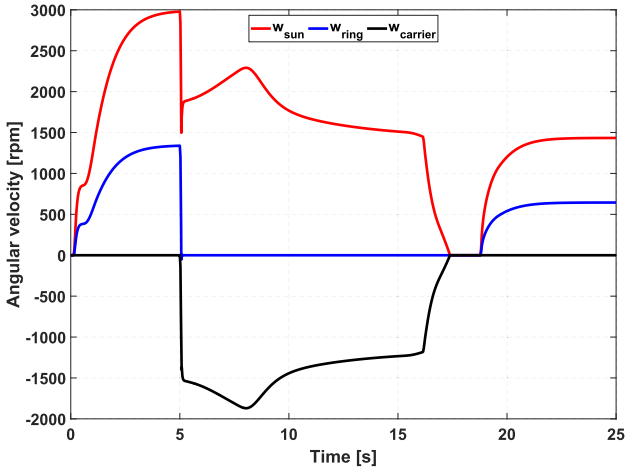

FIGURE 25. Angular velocities of the planetary gears.

nature during the entire operation, including the gear mode changes.

From the time instant the ring gear goes to rest till the end of the *Reverse* mode, the carrier's angular velocity is the same as that of the sun multiplied by $-\frac{272}{675}r_{rev}$, as can be observed from the figure. For disengaging the reverse clutch, its outflow solenoid is turned ON at 18 seconds, as shown in Fig. 22. Around 18.8 seconds, the reverse clutch gets fully disengaged, and the sun and ring gear starts rotating freely while the carrier remains at rest. Then, the algebraic state switches to ω_{rg} from ω_c and the system dynamics along with it.

To visualize these features better, we developed an animated representation which can be found in doi.org/10.6084/m9.figshare.17951144.

XIII. CONCLUSION

In this work, 1) a dynamic model for a double pinion planetary gearbox, 2) a model of a push belt CVT is presented, 3) a dynamic model of a lockup torque converter, 4) a model for a directional control valve, and 5) an aggregated model for an ICE vehicle's powertrain comprising a CVT is presented. The planetary gear system is modeled as a switching DAE system. It is shown that by incorporating the forward and reverse clutch dynamics with the gearbox model, the transient characteristics of the gear system can be captured. Contrary to shifting gear ratios to discrete values instantaneously, our modeling approach helps retain the continuity of the gear ratios in the powertrain. Additionally, this technique lowers the significant stiffness in the differential equations of the entire system dynamics that arise due to discontinuous discrete gear ratios. It is shown how modeling the CVT as a DAE system allows to integrate the variator kinematics with the dynamics of the CVT components. The response of the torque converter shows the model preserves the continuity in the angular velocities of the torque converter components during the locking and unlocking of the torque converter. Thus the transient effects in the powertrain during these events are duly captured. It is shown how the modeling approach for the DCVs helps to operate the DCVs with any spool displacement, thereby making the model fit for precise and accurate control. Moreover, the DCV model captures the partial flows during the transient stages and retains the continuity of the hydraulic pressures in the pulley cylinders and the associated hydraulic lines. These models are combined with models of other powertrain components to obtain an aggregated powertrain model. Models of other vehicle systems can be combined with this powertrain model, and a complete vehicle model can be obtained to develop an autonomous controller.

The response of the powertrain model is studied using three case study examples and is found to be consistent with the expected behaviour. The case studies illustrate the behaviour of the proposed models under different traffic scenarios, stop-and-go behaviour, and reverse motion. The utility of the planetary gear model to operate the powertrain in *Drive-Neutral-Reverse* gear modes and in preserving the gear ratios' continuity during changes in gear modes are shown. The CVT controller can also be used to compare the response of a CVT with other automatic transmissions. Also, the control strategy can be followed in designing CVT controllers to operate the CVT at specific values of gear ratios.

Furthermore, the model's modularity allows using the individual subsystems' model in other combinations of powertrains. For example, the CVT model can be used in modeling a Hybrid powertrain, the model of the planetary gears can be used to model multi-stage automatic transmission. The proposed models can be combined with other vehicle subsystems such as steering, chassis dynamics, etc. The combined model can be used with semi-autonomous controllers and driver models for generating vehicle behaviour to analyze the dynamics of vehicle mobility networks comprising autonomous, semi-autonomous, and human-driven vehicles.

REFERENCES

[1] *Taxonomy and Definitions for Terms Related to Driving Automation Systems for on-Road Motor Vehicles*, On-Road Automated Driving (ORAD) Committee, SAE Int., Warrendale, PA, USA, Apr. 2021, doi: 10.4271/J3016_202104.
[2] J.-F. Bonnefon, A. Shariff, and I. Rahwan, "The social dilemma of autonomous vehicles," *Science*, vol. 352, no. 6293, pp. 1573–1576, 2016, doi: 10.1126/science.aaf2654.
[3] D. Hrovat and W. Tobler, "Bond graph modeling and computer simulation of automotive torque converters," *J. Franklin Inst.*, vol. 319, no. 1, pp. 93–114, 1985, doi: 10.1016/0016-0032(85)90067-5.
[4] D. Cho and J. K. Hedrick, "Automotive powertrain modeling for control," *J. Dyn. Syst., Meas., Control*, vol. 111, no. 4, pp. 568–576, Dec. 1989, doi: 10.1115/1.3153093.
[5] A. Balachandran and J. C. Gerdes, "Designing steering feel for steer-by-wire vehicles using objective measures," *IEEE/ASME Trans. Mechatronics*, vol. 20, no. 1, pp. 373–383, Feb. 2015.
[6] H. B. Pacejka and E. Bakker, "The magic formula tyre model," *Vehicle Syst. Dyn.*, vol. 21, no. S1, pp. 1–18, 1992, doi: 10.1080/00423119208969994.
[7] D. Bhattacharjee, P. Bhola, and P. K. Dan, "A heuristic synthesis of multistage planetary gearbox layout for automotive transmission," *Proc. Inst. Mech. Eng., K, J. Multi-body Dyn.*, vol. 233, no. 2, pp. 336–347, Jun. 2019, doi: 10.1177/1464419318759893.
[8] A. Kahraman, "Planetary gear train dynamics," *J. Mech. Des.*, vol. 116, no. 3, pp. 713–720, Sep. 1994, doi: 10.1115/1.2919441.
[9] C.-J. Bahk, "Analytical study on nonlinear dynamics of planetary gears," Ph.D. dissertation, Dept. Mech. Eng., Ohio State Univ., Columbus, OH, USA, 2012.
[10] G. Carbone, L. Mangialardi, B. Bonsen, C. Tursi, and P. A. Veenhuizen, "CVT dynamics: Theory and experiments," *Mech. Mach. Theory*, vol. 42, no. 4, pp. 409–428, Apr. 2007, doi: 10.1016/j.mechmachtheory.2006.04.012.
[11] E. Shafai, M. Simons, U. Neff, and H. P. Geering, "Model of a continuously variable transmission," *Adv. Automot. Control*, vol. 28, no. 1, pp. 105–113, 1995, doi: 10.1016/S1474-6670(17)45681-3.
[12] T. Ide, A. Udagawa, and R. Kataoka, "A dynamic response analysis of a vehicle with a metal V-belt CVT," *JSAE Rev.*, vol. 16, no. 2, p. 215, 1995.
[13] M. Pesgens, B. Vroemen, B. Stouten, F. Veldpaus, and M. Steinbuch, "Control of a hydraulically actuated continuously variable transmission," *Vehicle Syst. Dyn.*, vol. 44, no. 5, pp. 387–406, May 2006, doi: 10.1080/00423110500244088.
[14] S. van der Meulen, R. van Iperen, B. de Jager, F. Veldpaus, F. van der Sluis, and M. Steinbuch, "A validated modular model for hydraulic actuation in a pushbelt continuously variable transmission," *J. Dyn. Syst., Meas., Control*, vol. 133, no. 4, pp. 1–15, Jul. 2011, doi: 10.1115/1.4003207.
[15] F. van der Sluis, "A new pump for CVT applications," SAE Int., Warrendale, PA, USA, Tech. Rep. 2003-01-3207, Oct. 2003, doi: 10.4271/2003-01-3207.
[16] J. Zhang, D. Wang, B. Xu, Z. Lu, M. Gan, and Q. Su, "Modeling and experimental validation of the time delay in a pilot operated proportional directional valve," *IEEE Access*, vol. 6, pp. 30355–30369, 2018.
[17] J. Deur, D. Hrovat, and J. Asgari, "Analysis of torque converter dynamics," in *Proc. ASME Int. Mech. Eng. Congr. Expo.*, in Dynamic, Systems and Control, vol. 36290, 2002, pp. 757–765, doi: 10.1115/IMECE2002-32156.
[18] J. Deur, J. Petric, and D. Hrovat, "Recent advances in control-oriented modeling of automotive power train dynamics," *IEEE/ASME Trans. Mechatronics*, vol. 11, no. 5, pp. 513–523, Oct. 2006.
[19] S. Iqbal, F. Al-Bender, A. P. Ompusunggu, B. Pluymers, and W. Desmet, "Modeling and analysis of wet friction clutch engagement dynamics," *Mech. Syst. Signal Process.*, vols. 60–61, pp. 420–436, Aug. 2015. [Online]. Available: https://www.sciencedirect.com/science/article/pii/S0888327015000291

[20] J. Deur, J. Petric, J. Asgari, and D. Hrovat, "Modeling of wet clutch engagement including a thorough experimental validation," SAE Int., Warrendale, PA, USA, Tech. Rep. 2005-01-0877, Apr. 2005, doi: 10.4271/2005-01-0877.
[21] Y. Yuan, E. A. Liu, J. Hill, and Q. Zou, "An improved hydrodynamic model for open wet transmission clutches," *J. Fluids Eng.*, vol. 129, no. 3, pp. 333–337, Mar. 2007, doi: 10.1115/1.2427088.
[22] X. Song and Z. Sun, "Pressure-based clutch control for automotive transmissions using a sliding-mode controller," *IEEE/ASME Trans. Mechatronics*, vol. 17, no. 3, pp. 534–546, Jun. 2012.
[23] X. Song, M. A. M. Zulkefli, Z. Sun, and H.-C. Miao, "Automotive transmission clutch fill control using a customized dynamic programming method," *J. Dyn. Syst., Meas., Control*, vol. 133, no. 5, Sep. 2011, Art. no. 054503, doi: 10.1115/1.4003797.
[24] D. R. Grandall, "The performance and efficiency of hydraulic pumps and motors," Ph.D. dissertation, Dept. Mech. Eng., Univ. Minnesota Digit. Conservancy, Minneapolis, MN, USA, 2010. [Online]. Available: http://hdl.handle.net/11299/59818
[25] M. Jelali and A. Kroll, *Hydraulic Servo-Systems: Modelling, Identification and Control*. London, U.K.: Springer, 2012, doi: 10.1007/978-1-4471-0099-7.
[26] P. Naseradinmousavi and C. Nataraj, "Nonlinear mathematical modeling of butterfly valves driven by solenoid actuators," *Appl. Math. Model.*, vol. 35, no. 5, pp. 2324–2335, May 2011, doi: 10.1016/j.apm.2010.11.036.
[27] E. Hendricks and S. C. Sorenson, "Mean value modelling of spark ignition engines," SAE Int., Warrendale, PA, USA, Tech. Rep. 900616, Feb. 1990, doi: 10.4271/900616.
[28] E. D. Ruiz-Rojas, J. L. Vazquez-Gonzalez, R. Alejos-Palomares, A. Z. Escudero-Uribe, and J. R. Mendoza-Vázquez, "Mathematical model of a linear electric actuator with prosthesis applications," in *Proc. 18th Int. Conf. Electron., Commun. Comput. (Conielecomp)*, Mar. 2008, pp. 182–186.
[29] J. C. Gerdes and J. Hadrick, "Brake system modeling for simulation and control," *J. Dyn. Syst., Meas., Control*, vol. 121, no. 3, pp. 496–503, 1999, doi: 10.1115/1.2802501.
[30] S. van der Meulen, B. de Jager, F. Veldpaus, E. van der Noll, F. van der Sluis, and M. Steinbuch, "Improving continuously variable transmission efficiency with extremum seeking control," *IEEE Trans. Control Syst. Technol.*, vol. 20, no. 5, pp. 1376–1383, Sep. 2012.
[31] R. J. Pulles, B. Bonsen, M. Steinbuch, and P. A. Veenhuizen, "Slip controller design and implementation in a continuously variable transmission," in *Proc. Amer. Control Conf.*, vol. 3, 2005, pp. 1625–1630.
[32] C. Lazar, F. C. Caruntu, and A. E. Balau, "Modelling and predictive control of an electro-hydraulic actuated wet clutch for automatic transmission," in *Proc. IEEE Int. Symp. Ind. Electron.*, Jul. 2010, pp. 256–261.

SUBHADEEP KUMAR received the bachelor's degree in electronics and telecommunication engineering from the Indian Institute of Engineering Science and Technology, Shibpur, West Bengal, India, in 2014. He is currently pursuing the Ph.D. degree in control and optimization with the Indian Institute of Technology Madras, Chennai, India. His current research interests include automotive control, autonomous driving, automotive sensing, vehicular traffic, and transportation networks.

RAMKRISHNA PASUMARTHY (Member, IEEE) received the Ph.D. degree in systems and control from the University of Twente, Enschede, The Netherlands, in 2006. He is currently an Associate Professor with the Department of Electrical Engineering, Indian Institute of Technology Madras, Chennai, India, where he is also associated with the Robert Bosch Center for Data Science and Artificial Intelligence. He also held visiting positions with the Stanford University School of Medicine, Stanford, CA, USA. His research interests include modeling and control of complex, physical, and networks systems with applications to power, traffic, and brain networks; and identification and control and resource optimization in (cloud) computing systems.

NIRAV P. BHATT (Member, IEEE) received the master's degree in chemical engineering from the Indian Institute of Technology Madras, Chennai, India, and the Doctor of Science (D.Sc.) degree in control engineering and data science from EPFL, Switzerland. Currently, he is an Assistant Professor with the Biotechnology Department, Indian Institute of Technology Madras. He is also associated with the Robert Bosch Center for Data Science and Artificial Intelligence. His research interests include modeling and control of biological, chemical, and infrastructure networks, and AI/ML techniques for analysis of biological; and infrastructure networks data.